Electrocorticographic dissociation of alpha and beta rhythmic activity in the human sensorimotor system

Arjen Stolk[1,2], Loek Brinkman[3], Mariska J. Vansteensel[3], Erik Aarnoutse[3], Frans S. S. Leijten[3], Chris H. Dijkerman[4], Robert T. Knight[1], Floris P. de Lange[2], Ivan Toni[2]

[1]Helen Wills Neuroscience Institute, University of California, Berkeley, CA, USA;

[2]Donders Institute for Brain, Cognition, and Behaviour, Radboud University, Nijmegen, The Netherlands;

[3]UMC Utrecht Brain Center, Department of Neurology and Neurosurgery, UMC Utrecht, Utrecht, The Netherlands;

[4]Helmholtz Institute, Experimental Psychology, Utrecht University, Utrecht, The Netherlands

Impact statement: Direct cortical recordings in humans link the spectral structure of local field potentials to inhibition/disinhibition mechanisms coordinating sensorimotor neuronal populations during movement selection.

Abstract This study uses electrocorticography in humans to assess how alpha- and beta-band rhythms modulate excitability of the sensorimotor cortex during movement selection, as indexed through a psychophysically-controlled movement imagery task. Both rhythms displayed effector-specific modulations, tracked spectral markers of action potentials in the local neuronal population, and showed spatially systematic phase relationships (traveling waves). Yet, alpha- and beta-band rhythms differed in their anatomical and functional properties, were weakly correlated, and traveled along opposite directions across the sensorimotor cortex. Increased alpha-band power in the somatosensory cortex ipsilateral to the selected arm was associated with spatially-unspecific inhibition. Decreased beta-band power over contralateral motor cortex was associated with a focal shift from relative inhibition to excitation. These observations indicate the relevance of both inhibition and disinhibition mechanisms for precise spatiotemporal coordination of neuronal populations during movement selection. Those mechanisms are implemented through the substantially different neurophysiological properties of sensorimotor alpha- and beta-band rhythms.

Introduction

To control a movement, specific neuronal populations supporting particular features of that movement need to be facilitated while other populations need to be suppressed (Ebbesen and Brecht, 2017; Greenhouse et al., 2015; Mink, 1996). Both operations need to be organized in a precise spatiotemporal pattern, such that the demands of coordinating body segments for movement are dynamically solved through the selective excitation and inhibition of relevant and irrelevant sensorimotor neuronal populations (Bruno et al., 2015; Dombeck et al., 2009; Graziano, 2016; Shenoy et al., 2013). One putative mechanism through which this sensorimotor coordination is implemented is the rhythmic modulation of neuronal local field potentials in the alpha (8 - 12 Hz) and beta (15 - 25 Hz) frequency range (Brovelli et al., 2004; Pfurtscheller and Berghold, 1989; Picazio et al., 2014; van Wijk et al., 2012).

Neuronal local field potentials in the sensorimotor cortex are organized in two prominent spectral clusters, alpha- and beta-band rhythms, known to be relevant for movement selection and to differ across several features. For instance, there are differences in the cortico-subcortical loops supporting alpha- and beta-band rhythms (Bastos et al., 2014; Leventhal et al., 2012; Schreckenberger et al., 2004; West et al., 2018), and only the latter rhythm has clear modulatory effects on corticospinal neurons (Baker et al., 1997; Madsen et al., 2019; Mima and Hallett, 1999; van Elswijk et al., 2010). Yet, the neurophysiological characteristics of alpha- and beta-band rhythms have often been studied by aggregating these two rhythms into the same (mu-) rhythm category (Cuevas et al., 2014; Hari, 2006; Miller et al., 2010), an approach often justified by the partial overlap in their spatial and spectral distributions (Bressler and Richter, 2015; Haegens et al., 2014; Salmelin and Hari, 1994; Szurhaj et al., 2003) and by the temporal correlation of their power envelopes (Carlqvist et al., 2005; de Lange et al., 2008; Tiihonen et al., 1989). By aggregating those rhythms, it has been recently shown that 4–22 Hz activity modulates high-frequency broadband power in primates' frontal cortex (Bastos et al., 2018; Johnston et al., 2019), and that 10-45 Hz activity is spatially organized in traveling waves (Rubino et al., 2006; Takahashi et al., 2015). It remains unclear, however, whether that aggregation could obscure differential contributions of those rhythms to movement selection. For instance, it is an open question whether alpha- and beta-band rhythms modulate the excitability of the same neuronal ensembles in the same direction when a movement is selected across the sensorimotor cortex (Brinkman et al., 2016, 2014).

Here we used direct recordings from the human cortical surface (electrocorticography, ECoG; Figure 1A) to assess the anatomical and functional specificity of alpha- and beta-band rhythms and their effects on the local excitability of sensorimotor neuronal ensembles during

performance of a task indexing movement selection. Local cortical effects were quantified through two complementary power-spectral metrics of excitability. First, we considered high-frequency (60 - 120 Hz) content in the ECoG signal, a mesoscale correlate of action potentials and dendritic currents in the local neural population (Leszczynski et al., n.d.; Manning et al., 2009; Miller et al., 2009; Ray and Maunsell, 2011; Rich and Wallis, 2017). Second, we considered the slope of the power-spectral density function ($1/f$ slope), a putative summary index of synaptic excitation/inhibition balance (Gao et al., 2017). Furthermore, rather than assuming that alpha- and beta-band rhythms are spatially stationary across the sensorimotor cortex (Brinkman et al., 2016, 2014), we examined the spatiotemporal distribution of the two sensorimotor rhythms and their cortical effects through two complementary analyses. First, we considered the organization of spatially systematic phase relationships among rhythmic signals (traveling waves) across the sensorimotor cortex (Ermentrout and Kleinfeld, 2001; Muller et al., 2018). Second, we explored the spatiotemporal relation between rhythm strength and local cortical excitability through analysis of representational similarity between those spectral markers (Kriegeskorte et al., 2006).

This neurophysiological characterization of alpha- and beta-band rhythms is based on a principled differentiation of the two sensorimotor rhythms along spectral, anatomical, and movement-related dimensions. Spectrally, alpha- and beta-band signals were disambiguated from arrhythmic spectral components in each individual participant (Wen and Liu, 2015). This procedure increases spectral precision and physiological interpretability by controlling for the effects of task-related power-spectral $1/f$ modulations over those rhythms (He, 2014). Anatomically, the ECoG recordings were precisely registered to the cortical anatomy of each patient (Stolk et al., 2018), and sorted according to the sensorimotor responses evoked by electrical stimulation of the electrodes. Functionally, the movement-related specificity of alpha- and beta-band signals was experimentally controlled by using imagined movements psychophysically-matched to actual movements (Figure 1B, (Brinkman et al., 2014; Rosenbaum et al., 1995)). This procedure is grounded on the close correspondence between neural mechanisms of movement selection and motor imagery. Besides sharing motor control variables and sensitivity to biomechanical constraints (de Lange et al., 2006; Gentili et al., 2004; Vargas et al., 2004), movement selection and motor imagery evoke the same activity patterns in dorsal premotor cortex and in the subthalamic nucleus (Cisek and Kalaska, 2004; Kühn et al., 2006), leading to similar consequences on the excitability of the corticospinal system (Lebon et al., 2019). Moreover, using motor imagery increases functional interpretability by avoiding confounding execution-related somatosensory

reafference known to differentially affect post-movement power dynamics in the alpha- and beta-bands (Alayrangues et al., 2019; Jurkiewicz et al., 2006; Tan et al., 2016).

Results

Direct cortical recording during psychophysically-controlled movement imagery

Neurosurgical epilepsy patients implanted with subdural grid and strip electrode arrays for clinical diagnostic purposes performed up to three sessions of a movement imagery task where they imagined how to grasp an object with either their left or right hand. Eleven patients participated, eight with left hemisphere arrays, and three with arrays on the right (see overlay on a template brain in Figure 1A). Two participants experienced difficulties adhering to the task instructions and were excluded from further analysis.

The motor imagery task involved 60 trials per session. Each trial started with the presentation of a black-white cylinder on a computer screen. Participants imagined how to grasp the middle-third of that cylinder with either their left or right hand, in alternating blocks of 10 trials (Figure 1B). After a fixed amount of time, a response screen appeared where the participants indicated whether their thumb was on the black or the white part of the cylinder at the end of the imagined movement. The response screen consisted of two squares on the horizontal plane (one black and one white), where participants indicated 'black' or 'white' by pressing the corresponding button using their left or right thumb on a button box that they held with both hands. The relative location of the black and white squares on the screen was pseudo-randomized across trials to prevent the preparation of the thumb response during the simulation of the grasping movements.

The task was designed to assess whether participants produced imaginary movements conforming to the biomechanical constraints of the corresponding real movements. On each trial, the cylinder was pseudo-randomly tilted according to 1 of 15 possible orientations, spanning 0 to 360°. This task manipulation resulted in trials affording both overhand and underhand grasping, and trials that afforded grasping in a single manner only due to biomechanical constraints of the hand. As seen in Figure 1C, the preferred manner in which participants imagined grasping the cylinder (thumb on black or white part) depended on the orientation of the cylinder and followed the biomechanical constraints of the body. This is supported by a psychophysical analysis showing that a sine-wave fit to the over-/underhand data points explained 81 ± 4 % of the variance in the left-hand condition (M ± SEM; $t(8) = 18.4$, $p < 0.001$) and 76 ± 4 % in the right-hand condition ($t(8) = 21.6$, $p < 0.001$), consistent with the prediction of two orientation-dependent switch points in each hand's response curve, i.e., the 50% crossings in Figure 1C (Brinkman et al., 2014).

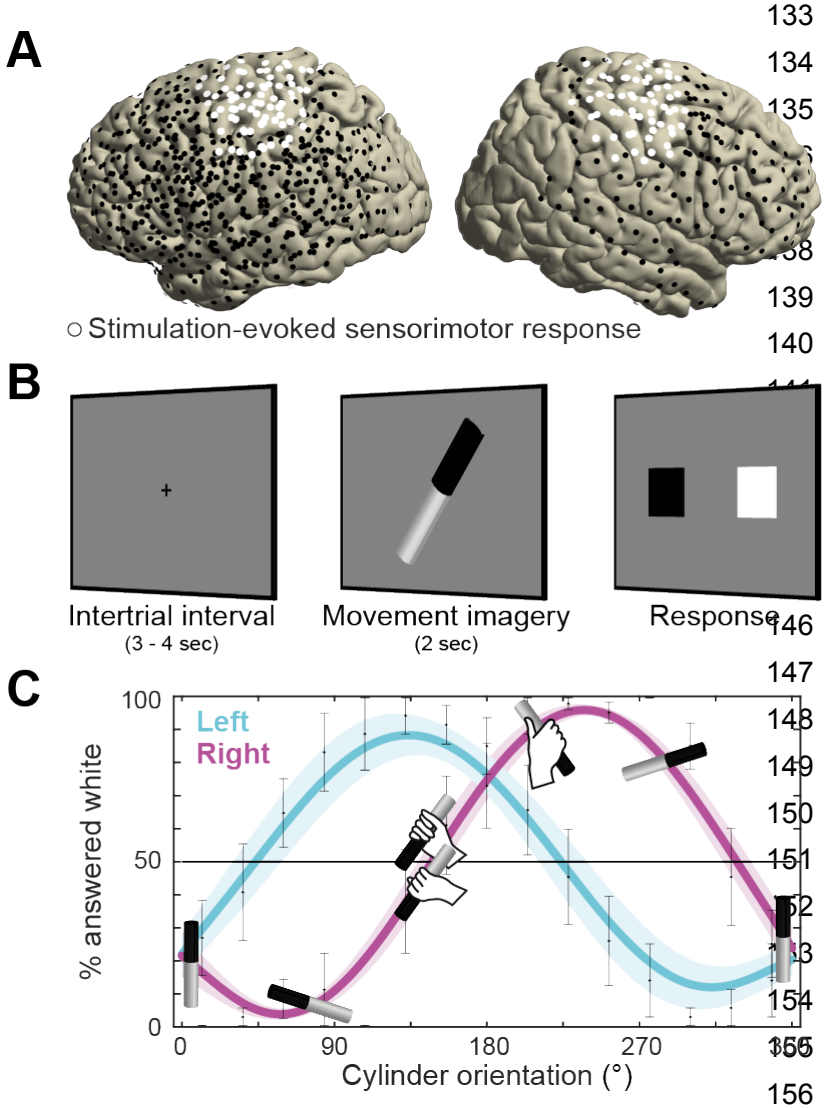

Figure 1. Recording electrode locations and movement imagery task. (**A**) Neural signals were recorded from the cortical surface of eleven epilepsy patients that were implanted with subdural electrode grids and strips. The electrode locations of all participants are overlaid on a template brain (black markers). Electrodes resulting in either a somatomotor or somatosensory response in the upper limb upon electrical stimulation are highlighted in white. (**B**) Participants imagined grasping the middle-third of a black-white cylinder with either their left or right hand. At the response screen, they indicated whether their thumb was on the black or the white part of the cylinder at the end of the imagined movement. (**C**) The preferred manner in which the cylinder was grasped (thumb on black or white part, related to overhand vs. underhand grasping) was modulated as a function of the cylinder's orientation and differed for the left and right hand. Error bars indicate M ± SEM over nine participants. Lines and shaded areas indicate M ± SEM of sine-wave fits to individual over-/underhand data points.

Eight out of nine participants additionally completed a control task that used the same visual input and response contingencies as the motor imagery task, but where no imagery was required. In the control task, the surface areas of the cylinder differed slightly across trials, e.g., 54% black and 46% white, and participants reported which side of the black-white cylinder was larger. This allowed correcting for neural changes unrelated to the movement imagery process,

such as those evoked by the visual input. Participants performed the control task with high accuracy (99.4 ± 0.3 % correct, M ± SEM).

In the following sections, we first characterize the anatomical distribution and task-related temporal profile of neuronal ensembles supporting alpha- and beta-band rhythms across the sensorimotor cortex, as well as the functional consequences of electrical stimulation of those ensembles. Afterward, we assess the influence of those rhythms on the spatiotemporal pattern of sensorimotor excitability during the selection of a movement and the spatiotemporal organization of those rhythms across the sensorimotor cortex.

Alpha- and beta-band rhythms build on anatomically distinct neuronal ensembles

Neuronal ensembles producing sensorimotor alpha- and beta-band rhythms across the human sensorimotor cortex were isolated with a four-step procedure. The goal of the procedure is to characterize the spatial distribution of rhythmic and spectrally homogeneous neural activity in sensorimotor areas in each participant's subdural grid and strip electrode arrays.

First, for each participant, we selected electrodes that upon electrical stimulation yielded somatomotor or somatosensory responses of the upper limb contralateral to the cortical grid (i.e., twitches, movements, tingling of fingers, hand, wrist, arm, or shoulder). This procedure identified cortical regions supporting sensorimotor components of movement (white electrodes in Figure 1A, 2A). Seven out of nine participants showed such responses, indicating sensorimotor coverage in these participants. Second, we used irregular-resampling auto-spectral analysis (IRASA, (Wen and Liu, 2015)) of the neural signal recorded at the stimulation-positive electrodes. This procedure isolated specific rhythmic activity embedded in the concurrent broadband $1/f$ modulations. Third, mean and full-width at half-maximum of alpha and beta spectral distributions were defined for each participant using a Gaussian model (red and blue areas of the power-spectra in Figure 2A). This adaptive approach (Supplemental Data) avoids having to rely on canonical frequency bands that may not accurately capture the neural phenomena of interest in each individual (Haegens et al., 2014; Szurhaj et al., 2003). Five out of seven participants had a rhythmic power-spectral component that overlapped with the 8 - 12 Hz alpha frequency range, one had a rhythmic component below that range, and all seven had a rhythmic component that overlapped with the 15 - 25 Hz beta range (Figure S1). Participant S7 exhibited only a single rhythmic component (in the beta frequency range) and was excluded from further analysis. On average, the remaining six participants' alpha and beta frequency bands were centered on 7.4 ± 0.7 and 16.9 ± 1.1 Hz (M ± SEM), respectively. Fourth, we localized cortical sites showing relative maxima in alpha and beta

power. We selected electrodes that exceeded the upper limit of the 99% confidence interval for absolute spectral power in the respective frequency band across all stimulation-positive electrodes defined by the first step. This analysis yielded 4.0 ± 1.2 alpha and 3.4 ± 0.8 beta peak activity electrodes for participants S1 - S5 (M ± SEM, red and blue electrodes in Figures 2A and S1). Due to limited sensorimotor coverage, the number of electrodes could not be narrowed down for participant S6, and the four stimulation-positive electrodes in this participant were used for the analysis of temporal dynamics only.

The cortical sites isolated through this principled four-step procedure had systematically different functional and anatomical properties. All 20 electrodes with alpha-band local maxima were located posterior to the central sulcus, $\chi^2(19) = 40$, $p < 0.001$ (pre vs. postcentral sulcus), see the red electrodes in Figure 2D. As seen in the same figure, the 17 blue electrodes with beta-band local maxima were localized to both sides of the central sulcus, $\chi^2(16) = 1.1$, $p = 0.3$ (7 pre- and 10 postcentral). Furthermore, only 7 out of 30 combined unique electrodes were local maxima for both sensorimotor rhythms, suggesting that alpha- and beta-band rhythms involve largely different neuronal ensembles, $\chi^2(29) = 17$, $p < 0.001$. On average, alpha- and beta-band local maxima were separated by 11.8 ± 2.2 mm (M ± SEM).

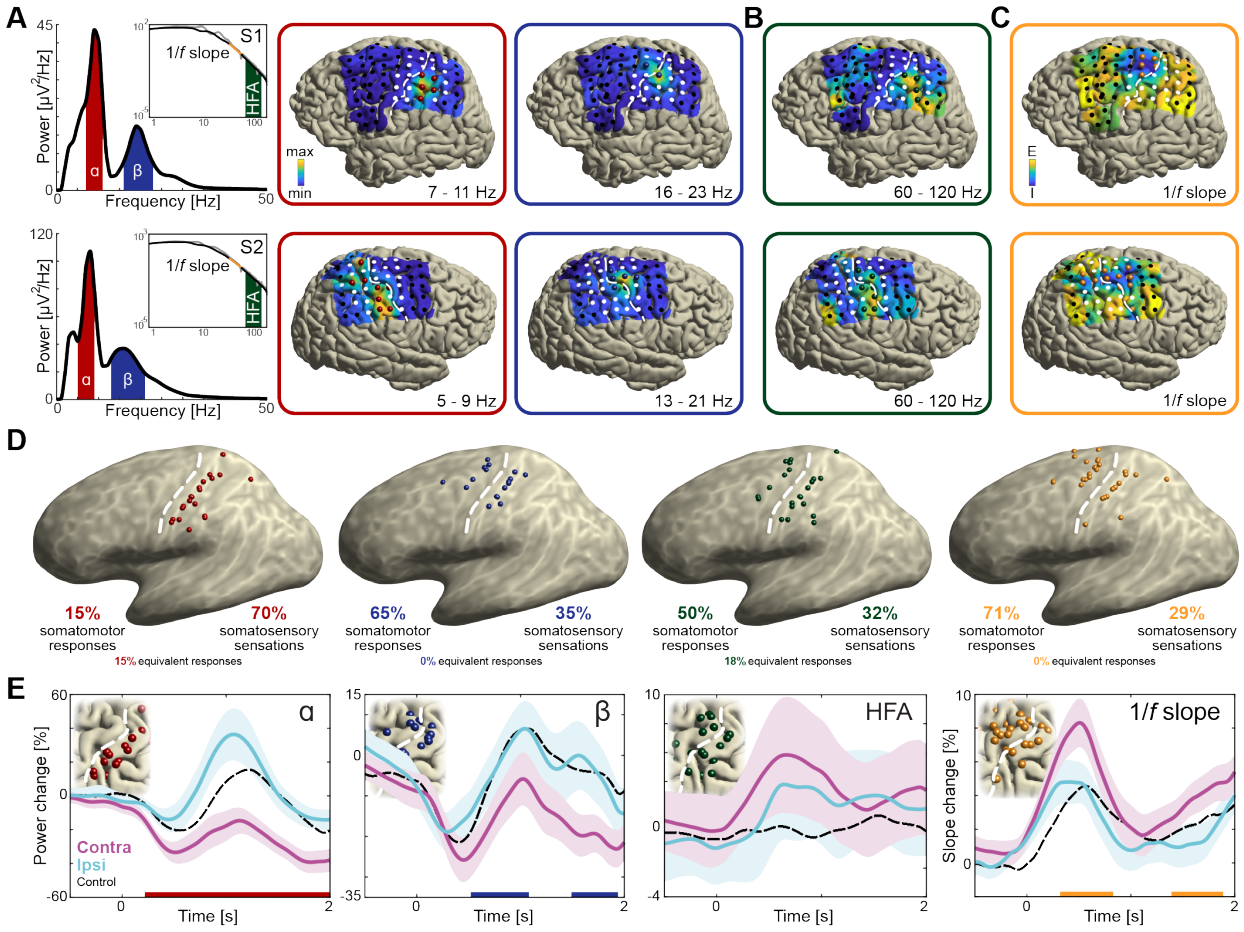

Figure 2. Anatomical and functional dissociation of sensorimotor alpha and beta. (**A**) Spectral and spatial distributions of alpha and beta rhythmic activity during imagined movement in two representative individuals. The insets show in log-log space the original power-spectra (in gray) and extracted arrhythmic 1/*f* content (black) that gave rise to the participant-specific rhythmic content shown in the main graph on the left. The color axes of the cortical maps run from minimum in blue to maximum absolute spectral power in yellow. White electrodes yielded somatomotor or somatosensory responses of the upper limb following electrical stimulation. Red and blue electrodes represent alpha- and beta-band local maxima across the sensorimotor cortex, respectively. (**B**) As the cortical maps in A, but for 60 to 120 Hz high-frequency arrhythmic content (HFA) of the ECoG signal. Green electrodes represent high-frequency-band local maxima across the sensorimotor cortex. (**C**) Ditto, but for the 1/*f* slope between 30 and 50 Hz, indicated by the orange graph sections in the insets of A. The 1/*f* slope is a putative power-spectral index of synaptic excitation/inhibition balance. Orange electrodes represent sensorimotor sites with relatively the strongest inhibition, i.e., the steepest slope. (**D**) Template brains showing the local maxima from five individuals visualized on the left hemisphere. Alpha is maximal at electrodes on the postcentral gyrus that yielded somatosensory sensations of the upper limb following electrical stimulation (red electrodes). In contrast, beta is strongest at electrodes placed over the central sulcus, with electrical stimulation yielding both movements

and somatosensory sensations (blue electrodes). White dashed lines indicate central sulci. (**E**) Temporal dynamics of power changes aggregated across the relevant local maxima during imagined movement of the contralateral or ipsilateral hand. Both neuronal ensembles producing alpha and beta rhythms showed effector-specific modulation during motor imagery, from 0 to 2 sec. Shaded areas indicate ±1 SEM. Colored bars along the x-axes indicate time intervals of statistically significant lateralization effects. Dashed black lines represent mean activity in the control task, for reference.

Alpha- and beta-band rhythms build on neuronal ensembles with different sensorimotor properties: effects of electrical stimulation

To test whether the neuronal ensembles generating alpha and beta rhythms had different functional properties, we probed the somatosensory and motor responses evoked by electrical stimulation of those ensembles. As indicated in Figure 2D, alpha electrodes yielded predominantly (14 out of 20 electrodes, 70%) somatosensory sensations of the contralateral upper limb following electrical stimulation, $\chi^2(19) = 12.4$, $p < 0.001$. Additionally, a subset of electrodes (3 out of 20, 15%) were part of equally many stimulation electrode pairs yielding both somatomotor and somatosensory responses. These observations suggest that alpha activity predominantly supports somatosensory components of a movement, in line with its anatomical distribution along the postcentral gyrus. By contrast, beta electrodes were marginally more likely (11 out of 17, 65%) to elicit a somatomotor than a somatosensory response of the upper limb following electrical stimulation, $\chi^2(16) = 2.9$, $p = 0.086$.

Alpha- and beta-band rhythms contribute to movement selection with different temporal dynamics

Since alpha and beta rhythms are anatomically and functionally separated at the cortical level, we asked whether the neuronal ensembles supporting the two sensorimotor rhythms provide different contributions to the selection of a movement. We considered the temporal dynamics of power changes in alpha- and beta-band rhythms, aggregated across the relevant local maxima. These temporal dynamics were highly correlated ($r = 0.7 \pm 0.1$, M ± SEM, $p < 0.002$) and both alpha- and beta-band power was more strongly attenuated for the hemisphere contralateral to the hand used in the imagined movement, see Figure 2E. Yet it can be seen from the same graph that alpha-band power increases in the (postcentral) cortex ipsilateral to the hand used for imagery, as compared to baseline levels (+34% between 910 and 1220 ms, $p < 0.05$; alpha-band power also decreased by 26% and 32% in the contralateral cortex between 170 and 850 ms and between 1230 and 2000 ms, respectively). In contrast, beta-band power decreases further in the (pre- and postcentral)

contralateral cortex (-21% between 150 and 760 ms vs. -13% in the ipsilateral cortex between -180 and 580 ms; there was another statistically significant change of -21% from baseline in the contralateral cortex between 1450 and 2000 ms). These differential power changes are robust on the single-trial level and, as seen in Figure S2, represented modulations of sustained rhythmic activity (Jones, 2016; Little et al., n.d.).

The temporal dynamics of these power changes are highly consistent with previous observations obtained from non-invasive electrophysiological recordings over sensorimotor cortex during performance of the same task, cf. Figure 3 in (Brinkman et al., 2014). In that magnetoencephalography (MEG) study, it was observed that as selection demands increased (when cylinder orientations afforded both over- and underhand grasping), alpha-band power increased in the sensorimotor cortex ipsilateral to the hand used for motor imagery, whereas beta-band power concurrently decreased in the contralateral sensorimotor cortex. We examined the alpha- and beta-band local maxima for similar effects, although the patients recorded in this ECoG study performed a substantially lower number of trials than the healthy participants of the MEG study (120 vs. 480, respectively). We defined high demand trials as trials involving cylinders oriented around the switch points estimated from each hand's response curve (range: three orientation bins per switch point, i.e., -24° to +24°). We compared alpha- and beta-band temporal dynamics on high demand trials with those on low demand trials, defined as trials with cylinder orientations orthogonal to the switch points and covering an equivalent range. It can be seen from Figure S3 that the direction of the effects is consistent with the previous MEG observations. There was a statistically significant decrease in contralateral beta rhythmic activity with increasing demand. However, the increase in ipsilateral alpha rhythmic activity did not pass the statistical threshold. Concerns regarding the limited number of trials refrained us from using the effects of task demand for further analyses.

Alpha- and beta-band rhythms arise from spatiotemporally unrelated neuronal ensembles

Since the temporal dynamics of alpha and beta rhythms aggregated across local maxima is functionally divergent, we asked whether that dissociation persists at more fine-grained levels of analysis across ECoG electrodes and trial-by-trial sensorimotor demands. First, we considered the temporal and spatial correlations between alpha- and beta-band power both between their respective local maxima (Figure 3A) and across the same functionally demarcated sensorimotor cortex (Figure 3B, C). It can be seen from the leftmost bars in these figures that alpha- and beta-band rhythms were temporally as well as spatially uncorrelated (all $BF_{01} > 1.56$ in favor of the null hypothesis of no correlation). This finding is a merit of the current procedure separating alpha and

beta rhythmic activity from concurrent 1/*f* modulations in the power spectrum, as power in the two frequency bands was correlated when this shared variance was not accounted for (Figure S4). Second, we considered the representational similarity of the temporal and spatial activity patterns evoked during movement imagery in the alpha- and beta-bands (Kriegeskorte, 2008). Instead of calculating direct correlations between the temporal dynamics or the spatial distribution of alpha- and beta-band power as above, this second-order correlation analysis quantifies the similarity in sensitivity to sensorimotor demands across trials, independently from the frequency-specific neural patterns evoked within a trial. Alpha- and beta-band rhythms showed weak resemblances in sensitivity to trial-by-trial demands, for both sensorimotor demands contained by temporal dynamics and activity patterns (Figure 3D-F, BF_{01}*s* of 1.06, 1.01, and 0.73, respectively). These relations between alpha- and beta-band effects indicate that the neuronal ensembles producing these two sensorimotor rhythms have no substantial spatiotemporal correspondences, neither within trials nor across trials.

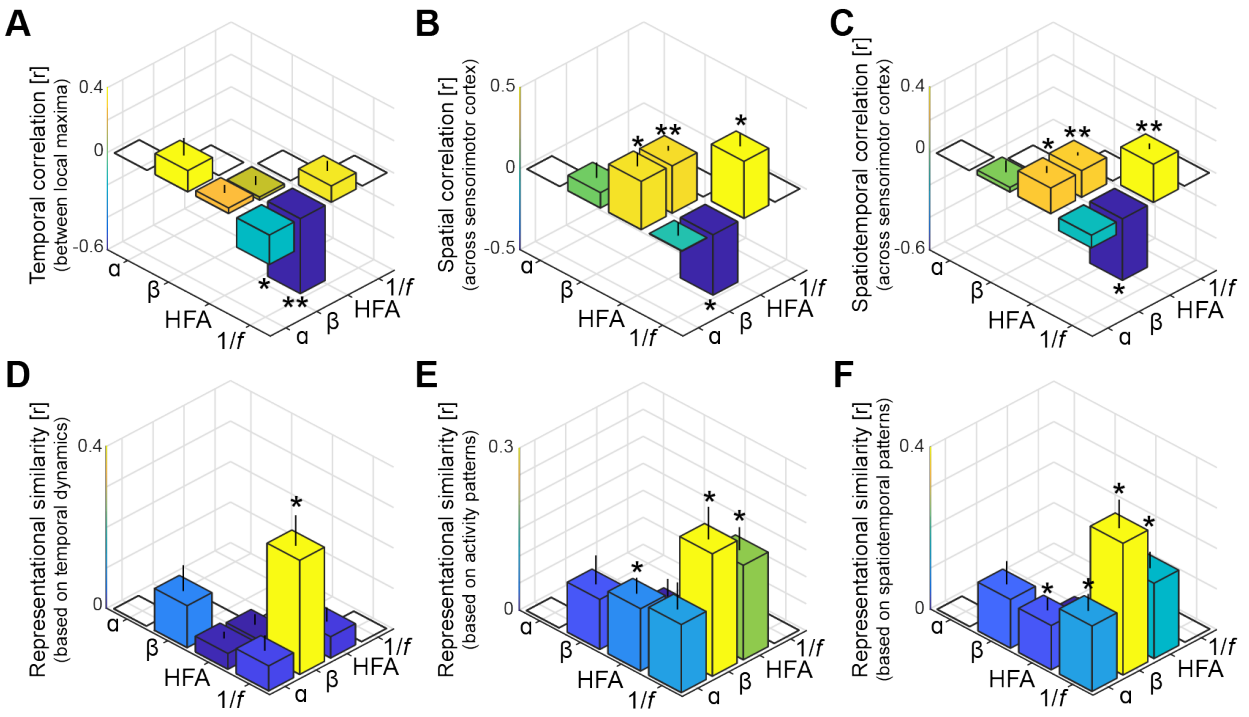

Figure 3. Spatiotemporal dissociation of sensorimotor alpha and beta. (**A** - **C**) Temporal, spatial, and spatiotemporal correlations between alpha, beta, high-frequency activity (HFA), and the 1/*f* slope. Alpha and beta rhythms were weakly correlated in time and space during movement. Both alpha and beta showed a positive relationship with high-frequency activity, yet only beta-band power closely tracked changes in the 1/*f* slope across sensorimotor cortex (B and C). *: $p < 0.05$; **: $p < 0.001$. (**D** - **F**) Alpha and beta rhythms showed weak similarity in sensitivity to sensorimotor demands across different movements. Echoing the

correlations shown in panels A to C, beta is largely sensitive to the same trial-by-trial demands as the 1/*f* slope, for both sensorimotor demands contained by temporal dynamics (D) and activity patterns (E and F).

Alpha- and beta-band rhythms have different influence on local excitability

The previous sections provide evidence for the notion that the neuronal ensembles generating alpha- and beta-band rhythms have different spatiotemporal characteristics during motor imagery, as well as different peripheral consequences following electrical stimulation. These observations confirm and qualify the findings of previous ECoG and SEEG reports on differences between alpha- and beta-band rhythms over the sensorimotor cortex (Brovelli et al., 2004; Crone et al., 1998; Jasper and Penfield, 1949; Saleh et al., 2010; Szurhaj et al., 2003; Toro et al., 1994; Vansteensel et al., 2013). Those clear differences between alpha- and beta-band rhythms raise the issue of understanding the functional consequences of those differences on the excitability of neuronal populations in the sensorimotor cortex during movement selection. We indexed those consequences through spectral markers of local population-level activity (arrhythmic high-frequency activity between 60 and 120 Hz (Manning et al., 2009; Miller et al., 2009; Ray and Maunsell, 2011)) and of local excitation/inhibition balance (steepness of the power-spectral 1/*f* slope, estimated between 30 and 50 Hz (Gao et al., 2017)). High-frequency activity showed spatial and temporal correspondences with both alpha- and beta-band rhythmic activity during movement selection (Figure 3B, C). This is also seen in the spatial distribution of local maxima in high-frequency activity (green electrodes in Figure 2D), which were localized to both sides of the central sulcus and involved neuronal ensembles producing alpha- or beta-band rhythmic activity (14/22: 4 producing alpha, 4 producing beta, 6 producing both alpha and beta, and 8 with no overlap). However, the lack of clear effector-specificity (Figure 2E) limits the functional relevance of this index.

Unlike high-frequency activity, the 1/*f* slope index showed clear functional specificity. This index was sensitive to the laterality of the effector involved in the motor imagery task (Figure 2E). This index was also spatially specific, with a focal reduction of excitation/inhibition ratio (i.e., steepest 1/*f* slopes, indicating stronger local inhibition) at electrodes placed over the central sulcus yielding predominantly somatomotor rather than somatosensory responses following electrical stimulation ($\chi^2(27) = 10.3$, $p < 0.002$; orange electrodes in Figure 2C, D). The spatial specificity of the 1/*f* slope index is further supported by a direct comparison with the spatial distribution of high-frequency activity: despite superficially similar distributions across the central sulcus (Figure 2D), only 3 out of 47 combined unique electrodes were both local maxima for high-frequency activity and local inhibition as indexed by the 1/*f* slope. One of the main findings of this study is that the 1/*f*

slope index had a differential relationship with the two sensorimotor rhythms. Figure 3A-C illustrates the reciprocal changes observed between beta-band activity and the $1/f$ slope during task performance. Namely, stronger reductions in beta-band power correlated with stronger increases in local excitability across sensorimotor cortex. Furthermore, electrodes with local maxima in beta-band activity and local inhibition were similarly distributed across the central sulcus, with a 59% (10/17) spatial correspondence. Given that both beta-band and $1/f$ slope indexes were similarly responsive to the laterality of the effector involved in the motor imagery task (Figure 2E), the spatiotemporal correspondence between beta-band rhythm and $1/f$ slope indicates that the stronger beta-band power reduction in the somatomotor cortex contralateral to the selected arm is associated with a relative disinhibition of somatomotor neuronal populations. This inference is supported and generalized by the representational similarity analyses of the temporal and spatial relations between those two spectral indexes evoked during movement imagery (Figure 3D-F). These analyses indicate that there is a robust spatiotemporal similarity across different imagined movements between beta-band power and $1/f$ slope, over and above the within-trial correlations captured in Figure 3A-C.

In contrast, the $1/f$ slope index had a different relationship with alpha-band responses to task demands. The putative index of excitation/inhibition balance was not spatially related to the alpha-band response (Figure 3B, C), with a 25% correspondence (5/20) between electrodes with local maxima in alpha-band activity and local inhibition. However, there was a significant temporal anti-correlation between local maxima of alpha-band power and $1/f$ slope (Figure 3A). This observation suggests that the stronger alpha-band power evoked in the somatosensory cortex ipsilateral to the selected arm (Figure 2E) is associated with a relative but spatially unspecific inhibition of the sensorimotor cortex. This inference is partially supported by the representational similarity analyses (Figure 3D-F). Although the trial-by-trial variation in spatiotemporal patterns of alpha-band power and $1/f$ slope is significantly related (Figure 3F), there are no clear similarities between those two spectral indexes when only temporal or spatial profiles are considered (Figure 3D, E).

Alpha- and beta-band rhythms propagate independently across sensorimotor cortex

The differential relation of alpha- and beta-band rhythms to (dis)inhibition of the sensorimotor cortex raises the issue of understanding whether that (dis)inhibition is propagated in a consistent spatiotemporal pattern. This possibility is functionally relevant: It has been suggested that there are consistent phase relationships among rhythmic cortical signals, organized in sparse traveling

waves that could facilitate sequences of activation in proximal-to-distal muscle representations in preparation for reaching behavior (Ermentrout and Kleinfeld, 2001; Muller et al., 2018). We explored this possibility by assessing the traveling wave characteristics of ECoG signals filtered at individual alpha- and beta-band frequencies and examining the functional relationship of those traveling waves with neuronal ensembles generating alpha and beta rhythms.

Visual inspection of single-trial filtered activity indicated that the phase of alpha- and beta-band signals varied systematically across the electrode array during motor imagery (Figure 4A). To quantitatively verify that rhythmic activity spatially progressed as traveling waves across sensorimotor cortex, we estimated spatial gradients of instantaneous rhythm phase computed using the Hilbert transform at each electrode across the recording array. These spatial gradients represent distance-weighted phase shifts between cortical signals at neighboring recording electrodes, where positive phase shifts correspond to signals that have covered a greater distance along the unit circle and thus lead the oscillation. To test whether the spatial gradients behaved like propagating waves at the single-trial level, we computed the phase-gradient directionality (PGD), a measure of the degree of phase-gradient alignment across an electrode array (Rubino et al., 2006). As seen through the small cone-shaped arrows positioned over each corresponding grid-electrode in Figure 4A, both alpha and beta phase gradients exhibited a higher degree of alignment across sensorimotor cortex than expected by chance (mean alpha PGD = 0.37, mean beta PGD = 0.35, $p <$ 0.001 in each patient for both alpha and beta, estimated from shuffled data). The traveling waves moved in a consistent direction across trials and over trial-time (circular histograms in Figure 4A; Rayleigh test of uniformity, $p < 10^{-18}$ in 5 out of 6 patients for alpha, $p < 10^{-91}$ in each patient for beta). Across participants, mean propagation speeds of the sensorimotor waves ranged between 5 and 9 cm/s for alpha and between 11 and 21 cm/s for beta (Figure 4B), consistent with previous reports of traveling beta waves in motor cortex (Rubino et al., 2006) and in the lower range of traveling alpha waves observed in posterior cortex (Bahramisharif et al., 2013; Halgren et al., 2017; Zhang et al., 2018). These observations corroborate and extend previous studies by showing that both alpha- and beta-band rhythms are organized in waves traveling across the sensorimotor cortex (Halgren et al., 2017; Takahashi et al., 2015; Zhang et al., 2018).

A novel finding of this study is that alpha and beta traveling waves propagate independently across sensorimotor cortex, as indicated by the distribution of propagation directions in individual participants (Figure 4A, Movies S1, S2) and by the mean probability distribution over participants (Figure 4C; mean Kullback-Leibler divergence = 0.10, $p < 0.001$ in each patient, estimated from shuffled data). Alpha waves propagated in a caudo-rostral direction, while beta waves advanced in

a rostro-caudal direction (Figure 4C, Figure S6). This analysis also revealed that electrodes sampling alpha- or beta-band rhythms with larger amplitudes were not sources or sinks of the alpha- or beta-traveling waves: Previously identified local maxima in alpha- and beta-band activity did not have a systematic phase advantage or delay in relation to other electrodes across the sensorimotor cortex (Figure 4A). Nevertheless, traveling-wave-like activity at these cortical sites was task-relevant, as indicated by an increase in directional consistency (DC) of those waves during movement imagery. Directional consistency measures the degree of consistency across trials in the phase-gradient direction (Zhang et al., 2018). As seen in Figure 4D, alpha rhythms propagated in a more consistent direction during imagined movement of the ipsilateral hand, while the propagation direction of beta rhythms became more consistent during imagined movement of the contralateral hand, as compared to baseline levels (see Figure S7 for the effects of task demand). Together, these observations indicate that the broader spatiotemporal context in which rhythmic cortical signals are embedded constitute an important component of movement selection, as indexed through motor imagery, and that this spatiotemporal organization differs for alpha and beta rhythms.

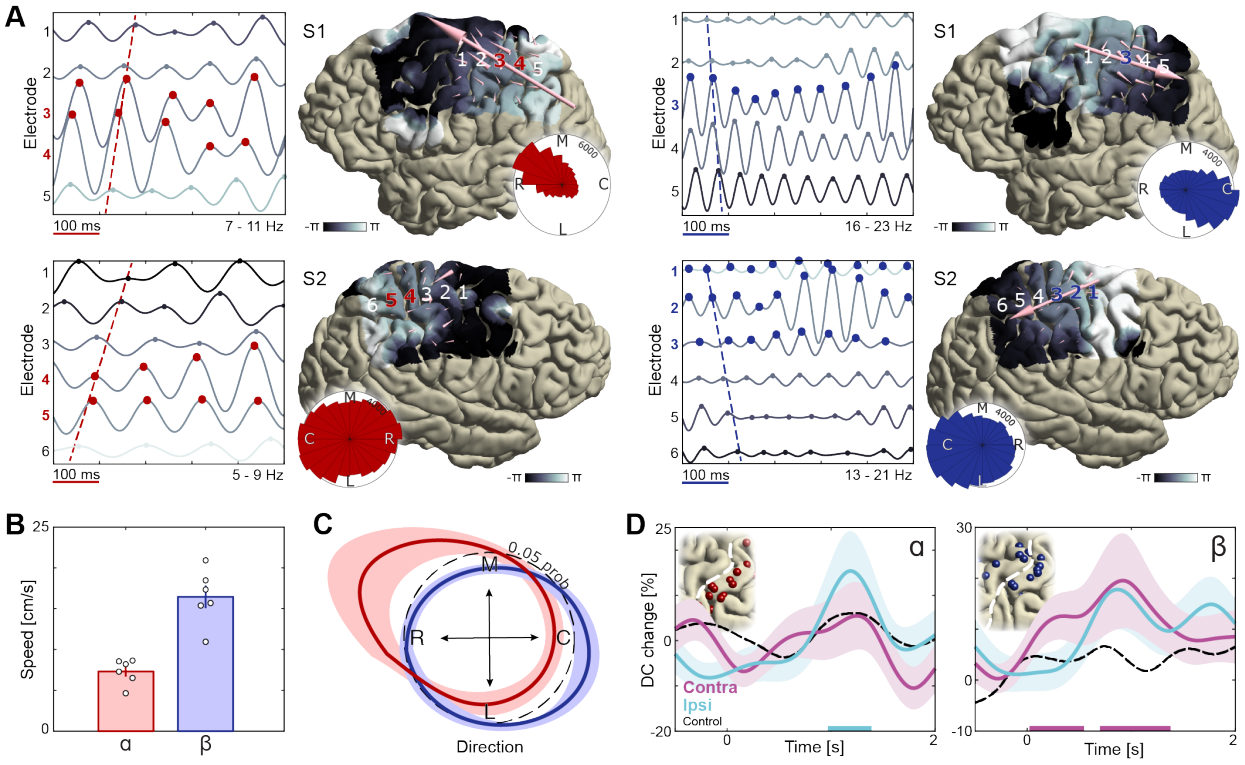

Figure 4. Dissociation of sensorimotor alpha and beta traveling waves. (**A**) Propagation of alpha and beta rhythmic activity during imagined movement in two representative individuals. Example cortical signals are of the same data segment in each participant but filtered at individual alpha and beta frequencies. Red and blue markers indicate electrodes previously identified as alpha- and beta-band local maxima, respectively. Cortical phase maps indicate the average phase at each cortical site relative to a central sensorimotor reference electrode. Small cone-shaped arrows indicate the mean propagation direction at each stimulation-positive electrode, with arrow size weighted by the local phase gradient magnitude. Large arrows indicate the mean propagation direction across sensorimotor cortex, with arrow size weighted by the alignment of sensorimotor gradients (phase gradient directionality, PGD). (**B**) Mean propagation speeds of traveling alpha and beta waves over participants. (**C**) Mean probability distribution of traveling wave direction over participants. Alpha rhythm propagation is maximal in a caudo-rostral direction (red distribution), while beta rhythms predominantly moved in a rostro-caudal direction (blue distribution). Dashed black circle represents a uniform distribution of propagation directions, for reference. (**D**) Alpha traveling waves propagated more consistently through alpha-band local maxima during imagined movement of the ipsilateral hand (directional consistency, DC). In contrast, beta waves traveled more consistently through beta-band local maxima during imagined movement of the contralateral hand. Colored bars along the x-axes indicate time intervals of statistically significant DC changes from baseline levels for the effector involved in the imagined movement.

Discussion

This ECoG study qualifies the spatiotemporal dynamics of alpha- and beta-band rhythms and their effects on the local excitability of sensorimotor neuronal ensembles during movement selection, in the context of a psychophysically-controlled motor imagery task. Rhythmic signals in the alpha- and beta-band were prominent in the patients' sensorimotor cortex, sustained across each trial, motorically relevant, and organized in spatially consistent waves of phase relationships traveling along opposite directions. In line with previous reports (Brinkman et al., 2014; Crone et al., 1998; de Lange et al., 2008; Miller et al., 2010), this study shows that the power envelopes of those two rhythms differentiated between imagined movements involving the contralateral or the ipsilateral hand. This study also confirms historical accounts by showing that alpha- and beta-band rhythms arise from anatomically and functionally distinct neuronal ensembles (Berger, 1938; Jasper and Penfield, 1949; Salmelin and Hari, 1994). Local maxima of alpha-band power were distributed on the postcentral gyrus, and electrical stimulation of those electrodes yielded somatosensory sensations of the upper limb. Sensorimotor beta was strongest at electrodes placed over the central sulcus, with electrical stimulation yielding both movements and somatosensory sensations. This study provides a novel piece of empirical evidence showing that sensorimotor alpha and beta rhythms have different neurophysiological properties, (dis)inhibiting different sensorimotor neuronal ensembles and dissociable functional components of movement selection. Namely, beta rhythmic activity closely tracked task-related modulations of the $1/f$ slope of the power-spectrum, an index of excitation/inhibition balance (Gao et al., 2017). The relation between beta and $1/f$ slope held across the spatial extent of the sensorimotor cortex, and within trials as well as across trials. When the $1/f$ slope transiently increased in somatomotor cortex during movement imagery, indicating a shift in balance from relative inhibition to excitation, beta rhythmic activity showed a focal reduction in signal strength. These findings suggest that imagery-related reduction in beta-band power, predominant over the somatomotor cortex contralateral to the selected arm, is associated with a relative disinhibition of somatomotor neuronal populations. This beta-band movement-related disinhibition was embedded within traveling waves moving along a rostro-caudal direction across the fronto-parietal cortex. There was also a relative increase in alpha-band power in the somatosensory cortex ipsilateral to the selected arm, an effect that was associated with a spatially unspecific inhibition of the sensorimotor cortex. This alpha-band inhibition was embedded within traveling waves along a caudo-rostral direction across the parieto-frontal cortex. We draw two main conclusions from these human neurophysiological observations. First, the evidence points to the relevance of both disinhibition and inhibition mechanisms for precise

spatiotemporal coordination of movement-related neuronal populations. Second, the evidence points to the dramatically different neurophysiological properties of sensorimotor alpha and beta rhythms, questioning the practice of aggregating those rhythms when studying cerebral function.

These findings emphasize how increased excitability of the sensorimotor cortex goes hand in hand with increased (and spatially widespread) inhibition. Speculatively, the spatiotemporal profile of increased excitability observed in the contralateral sensorimotor cortex might support the coordination of multiple sensorimotor cortical ensembles toward a movement-effective neural subspace (Elsayed et al., 2016; Shenoy et al., 2013), possibly implemented as dynamic modulations in direction- and frequency-dependent spatial arrangements of neuron receptor fields (Heitmann et al., 2013). Accordingly, beta waves in the motor cortex carry most movement-related information during the preparatory phase of a movement (Rubino et al., 2006). In contrast, the spatially unspecific inhibition of the ipsilateral sensorimotor cortex suggests that movement selection also requires suppression of task-irrelevant movements and in particular inhibition of their somatosensory correlates. It seems unlikely that this inhibitory effect was driven by somatosensory attention to the hand used during imagery since there were no lateralized power changes in the prestimulus baseline period, during which participants knew which hand they would use.

Interpretational issues

Previous micro-ECoG studies in non-human primates have shown systematic phase relationships between motor cortical signals less than a millimeter apart (Rubino et al., 2006; Takahashi et al., 2015). Here, we add to those findings by showing that alpha- and beta-band traveling waves propagate across the human sensorimotor cortex, independently. High-density laminar recordings of alpha and beta rhythmic activity might be able to test whether those rhythms propagate through different cortical layers (van Kerkoerle et al., 2014). Another possibility is that different cortico-thalamo-cortical and cortico-striatal-thalamo-cortical circuits lead to different alpha and beta traveling waves across the sensorimotor cortex (Bastos et al., 2014; Schreckenberger et al., 2004; West et al., 2018). The latter possibility could accommodate the observation that sources/sinks of the traveling waves were independent from electrodes sampling rhythms with larger amplitudes, and that there were no obvious phase-shifts between neighboring electrodes spanning a cortical fold. Large-scale corticothalamic recordings of alpha and beta waves might be able to define the precise mechanisms supporting those traveling waves over human sensorimotor cortex (Halgren et al., 2017).

Alpha- and beta-band rhythms are embedded within (but physiologically different from) arrhythmic broadband $1/f$ components of the signal, and their spectral distributions differ between individuals (a case in point is participant S7 lacking a rhythmic component in the alpha frequency range). Supplementary analyses indicate that ignoring those facts, as standard analytical pipelines do, led to strong but spurious correlation between alpha and beta power envelopes. Furthermore, the spatial differentiation between alpha- and beta-band cortical sources might prove too subtle for many non-invasive electrophysiological recordings (Brinkman et al., 2014; Fransen et al., 2016). These considerations might help to understand why those two sensorimotor rhythms are often aggregated into the same (mu-) rhythm category (Cuevas et al., 2014; Hari, 2006). Having shown that those two rhythms are anatomically and functionally distinct phenomena, it becomes relevant to know whether alpha and beta rhythms can also be systematically differentiated in other frontal brain regions (Bastos et al., 2018; Johnston et al., 2019).

Conclusions

The current findings indicate that alpha- and beta-band rhythms, besides having different anatomical distributions and traveling along opposite directions across the sensorimotor cortex, have different effects on cortical excitability. Increased alpha rhythmic activity in the somatosensory cortex ipsilateral to the selected arm is associated with spatially-unspecific cortical inhibition, whereas a reduction in beta rhythmic activity over contralateral motor cortex is associated with a spatially-focal shift in excitation/inhibition balance toward excitation. These findings increase our understanding of how cortical rhythms can mechanistically support the precise spatiotemporal organization of neuronal ensembles necessary for coordinating complex movements in humans.

Materials and methods

Participants

Eleven participants (7 males, 14 - 45 y of age) were implanted subdurally with grid and strip electrode arrays on the cortical surface to localize the seizure onset zone for subsequent surgical resection (Figure 1A). The electrode arrays (10 mm inter-electrode spacing, 2.3 mm exposed diameter; Ad-Tech, Racine, USA) were placed at the University Medical Center Utrecht, The Netherlands, on either right or left (8 cases) hemisphere. The number and anatomical location of the electrodes varied across participants, depending on the clinical considerations specific to each case (mean number of electrodes ± SEM: 81.3 ± 11.2). The sample size was determined by the availability of participants with (partial) electrode coverage of the central sulcus during the funding period of the project (four years). All participants had normal hearing and normal vision, and gave informed consent according to institutional guidelines of the local ethics committee (Medical Ethical Committee of the University Medical Center Utrecht), in accordance with the declaration of Helsinki. No seizures occurred during task administration. Two participants had difficulties adhering to the task instructions and frequently confused left- and right-hand conditions of the study. One of these participants had cavernous malformations in temporoparietal and frontal cortex. The other participant had experienced medical complications prior to task performance, leaving nine participants for analysis of the behavioral data. Two participants had no electrode coverage of upper-limb sensorimotor areas as indicated by electrocortical stimulation, leaving seven participants for analysis of the neural data.

Movement imagery task

Participants were positioned in a semi-recumbent position in their hospital bed and performed up to three sessions of a movement selection task (mean number of sessions ± SEM: 2 ± 0.2). In this task, participants imagined grasping the middle-third of a black-white cylinder with either their left or right hand (Figure 1B). The cylinder, tilted according to 1 of 15 possible orientations (24° apart, presented pseudo-randomly, size 17.5 x 3.5 cm), was presented on a gray background at the center of the computer screen that was placed within reaching distance in front of the participant. The duration for which the cylinder stayed on the screen was adjusted for each participant (2 - 5 sec) such that they could comfortably perform the task at a pace that suited their current physical and mental state. Next, a response screen appeared where the participants indicated whether their thumb was on the black or the white part of the cylinder at the end of the imagined movement. The response screen consisted of two squares on the horizontal plane (one black and one white), where

participants indicated 'black' or 'white' by pressing the corresponding button (left or right button) using the left or right thumb on a button box that they held with both hands. The order of the squares (black - left, white - right, or vice versa) was pseudo-random across trials to prevent the preparation of a response during the simulation of the grasping movements. After the response, a fixation cross appeared on the screen for 3 to 4 seconds (drawn randomly from a uniform distribution), after which the next trial started (intertrial interval). A single session consisted of 60 trials (10 minutes). The hand used to imagine the movement alternated every ten trials, prompted by a visual cue. The task exploited the fact that certain cylinder orientations afforded both overhand and underhand grasping, whereas other orientations afforded grasping in a single manner only, due to biomechanical constraints of the hand (Figure 1C). This task manipulation provided a test of participants' imagery performance as to whether their preferred manner for grasping the cylinder (thumb on black or white part) was modulated by biomechanical constraints, varying as a function of cylinder orientation and differing for the left and right hand.

Eight out of nine participants whose behavioral data are reported (5 out of 6 participants whose neural data are reported), completed a control task that used the same visual input and response contingencies, but where no imagery was required. In the control task, participants reported which side of the black-white cylinder was larger. That is, the surface areas differed slightly across trials, e.g., 54% black and 46% white, or vice versa. This allowed controlling for neural changes unrelated to the movement imagery process, such as those evoked by visual input during task performance.

ECoG acquisition and analysis

Electrophysiological data were acquired using the 128-channel Micromed recording system (Treviso, Italy, 22 bits), analog-filtered between 0.15 and 134.4 Hz, and digitally sampled at 512 Hz. During the recordings, participants were closely monitored for overt movements or distracting events. Epochs were these occurred were excluded from the analysis (6 ± 2% of the total amount of trials). Anatomical images were acquired using preoperative T1-weighted Magnetic Resonance Imaging (MRI, Philips 3T Achieva; Best, The Netherlands) and post-implantation Computerized Tomography (CT, Philips Tomoscan SR7000).

Data were analyzed using the open-source FieldTrip toolbox (Oostenveld et al., 2011), performing an integrated analysis of anatomical and electrophysiological human intracranial data. The procedure for the precise anatomical registration of the electrophysiological signal in each patient is described in detail elsewhere (Stolk et al., 2018). In brief, electrode locations in relation to

the brain's anatomy and the electrophysiological signal were obtained through identification of the electrodes in a post-implantation CT fused with the preoperative MRI. To correct for any displacement following implantation, the electrodes were projected to individually rendered neocortical surfaces along the local norm vector of the electrode grid (Hermes et al., 2010). We used FreeSurfer to extract anatomically realistic neocortical surfaces from each participant's MRI (Dale et al., 1999). FreeSurfer also allows registering the surfaces to a template brain on the basis of their cortical gyrification patterns (Greve et al., 2013). Using these surface registrations, we linked the electrodes from all participants to their template homologs, preserving the spatial relationship between cortical folding and electrode positions in each participant. This allowed for anatomically accurate comparison of local maxima in neural activity across participants.

The electrophysiological signals were visually inspected to ensure that they were free of epileptic activity or other artifacts (2 ± 2% of the total amount of trials excluded). Next, the data were digitally filtered (1 - 200 Hz bandpass, Butterworth, zero-phase forward and reverse), removed from power line noise components (50 Hz and harmonic band stop), and re-referenced to the common average of all channels to remove global noise shared across all channels from the potential in each channel. This produced reference-free cortical signals. We focused the analysis on the trial epochs during which the participants selected and imagined a movement, preceded by the appearance of the black-white cylinder. Using time-resolved Fourier analysis, we calculated spectral power with 1000 ms rolling Hanning-tapered windows at 50 ms increments. This produced time-frequency estimates up to 200 Hz with a 1 Hz spectral and a 20 Hz temporal resolution. Inter-session offsets in absolute spectral power were compensated for using linear regression analysis considering mean power across all time-frequency estimates in a session. For temporal dynamics analysis, the spectral data were expressed as percentage changes from bootstrapped spectral power during a pre-cylinder baseline interval (-750 to -500 ms to cylinder onset) and resampled to identical duration across participants (2 sec, after anti-aliasing). Differences in spectral power between the left- and right-hand conditions were evaluated using nonparametric cluster-based permutation statistics (two-sided dependent samples t-tests, $p < 0.05$, 10,000 randomizations (Maris and Oostenveld, 2007)), considering electrodes containing local maxima in neural activity as the unit of observation.

Spectral features extraction from sensorimotor cortex

Alpha and beta spectral and anatomical distributions were defined on a participant-by-participant basis, using a four-step procedure. First, electrodes covering cortical regions supporting

sensorimotor components of movement were identified using Electrocortical Stimulation Mapping (ESM, Micromed IRES 600CH), a standard clinical practice involving the pairwise electrical stimulation of adjacent cortical electrodes (typically at 50 Hz for 1 - 2 sec, with a 0.2 - 0.5 ms pulse duration and 1 - 4 mA intensity). Intensity of the stimulation was individually tailored, maximizing effect size while minimizing the occurrence of after-discharges. For each participant, we selected electrodes that were part of a stimulation electrode pair yielding motor or somatosensory responses of the upper limb contralateral to the cortical grid (twitches, movements, tingling of either fingers, hand, wrist, arm or shoulder).

Second, we used irregular-resampling auto-spectral analysis (IRASA, (Wen and Liu, 2015)) of the signal recorded at the stimulation-positive electrodes, allowing distinguishing rhythmic activity from concurrent power-spectral $1/f$ modulations. This technique virtually compresses and expands the time-domain data with a set of non-integer resampling factors prior to Fourier-based spectral decomposition, redistributing rhythmic components in the power-spectrum while leaving the arrhythmic $1/f$ distribution intact. Taking the median of the resulting auto-spectral distributions extracts the power-spectral $1/f$ component, and the subsequent removal of the $1/f$ component from the original power-spectrum offers a power-spectral estimate of rhythmic content in the recorded signal. It should be noted that the extracted spectral components no longer contain phase information and that their estimated magnitudes are susceptible to any phase relationships between the two components, as indicated by Equation 9 in the original paper (cf. two opposite-phase oscillations canceling out one another in the summed signal). As a consequence, power in the rhythmic component is negative at frequencies where the arrhythmic $1/f$ component exceeds power of the original power-spectrum. In cases where this happened (never at spectral peaks), we set power to zero to accommodate spectral curve fitting with exponential models in the next step.

Third, mean and full-width at half-maximum of alpha and beta spectral distributions were defined for each participant using a two-term or three-term Gaussian model, depending on the presence of a third low-frequency phenomenon in the rhythmic component of the power-spectrum (<5 Hz in two subjects, see power-spectra in Figure S1). This adaptive approach (Supplemental Data) avoids having to rely on canonical frequency bands that due in part to their narrowness may not accurately capture the neural phenomena of interest in each individual (Haegens et al., 2014; Szurhaj et al., 2003). On average, alpha and beta rhythmic activity were centered on 7.4 ± 0.7 and 16.9 ± 1.1 Hz, respectively. High-frequency neural activity was defined as activity within a broad 60 - 120 Hz range (Lachaux et al., 2012). Because of its hypothesized relationship with non-oscillatory population-level firing rate (Manning et al., 2009; Miller et al., 2009; Ray and Maunsell, 2011), we

687 estimated high-frequency activity using the arrhythmic 1/*f* component obtained above (see also
688 Figure S5 for an empirical argument). We additionally considered the slope of the arrhythmic 1/*f*
689 component, in log-log space. Computational modeling and local field potential recordings from rat
690 hippocampus suggest that the slope between 30 and 50 Hz is a power-spectral correlate of synaptic
691 excitation/inhibition balance, such that a steeper slope corresponds to greater inhibition in a
692 neuronal ensemble measured by the recording electrode. Notably, electrocorticography recordings
693 in the non-human primate brain indicate that the 1/*f* slope closely tracks the increase of inhibition
694 induced by propofol across space and time (Gao et al., 2017). Furthermore, recent intracranial
695 recordings in humans find that the slope between 30 and 50 Hz best predicts the depth of sleep and
696 anesthesia, more so than slow oscillatory power (Lendner et al., n.d.). We here assessed this
697 measure's potential for capturing movement initiation and suppression in human sensorimotor
698 cortex. Linear fits were used to estimate the steepness of the slope in the 30 - 50 Hz range (mean R^2
699 across all slope fits in each individual = 0.95 ± 0.00).
700 Fourth, for a fine-grained anatomical characterization, we localized all four sensorimotor
701 neuronal phenomena (alpha and beta rhythmic activity, high-frequency arrhythmic activity, and the
702 1/*f* slope) by selecting electrodes that exceeded the upper limit of the 99% confidence interval for
703 absolute spectral power in the respective frequency band across all stimulation-positive electrodes
704 defined by the first step (for the 1/*f* slope we used the lower limit of the confidence interval). This
705 analysis yielded 4 ± 1.2 alpha, 3.4 ± 0.8 beta, 4.4 ± 0.7 high-frequency, and 5.6 ± 1.4 1/*f* slope local
706 maxima in sensorimotor cortex for participants S1 - 5. Due to limited sensorimotor coverage, the
707 number of electrodes could not be narrowed down for participant S6, and all four stimulation-
708 positive electrodes were considered for further analysis involving temporal dynamics. Participant
709 S7 lacked a rhythmic power-spectral component in the alpha frequency range and was excluded
710 from further analysis.
711 We used chi-squared tests of electrode anatomical location and electrical stimulation
712 response type to assess differential basic sensorimotor properties of alpha and beta rhythms.
713 Anatomical location was defined as the electrode's spatial relationship to the central sulcus (pre vs.
714 postcentral sulcus), and response type as the sensorimotor nature of the evoked response following
715 electrical stimulation (motor response vs. somatosensory sensation).
716
717 **Spatiotemporal relations between spectral features**
718 To assess whether sensorimotor alpha, beta, high-frequency activity, and the 1/*f* slope shared
719 features during task performance, we performed a correlation analysis of their activity patterns

720 across time, space, as well as time and space combined. First, within-trial correlations of activity
721 dynamics between -750 and 2000 ms (relative to the onset of the visual stimulus) quantified the
722 temporal similarity between the four spectral features. These temporal correlations considered, for
723 each participant, mean activity across local maxima of each spectral feature (as identified with the
724 procedure described above). Each pair of spectral features produced a single correlation value per
725 trial. Second, a similar procedure was used to assess whether those spectral features involved
726 spatially overlapping or distinct neuronal ensembles across sensorimotor cortex. We considered
727 within-trial correlations of cortical activity patterns across stimulation-positive electrodes. In
728 contrast to temporal correlation, spatial correlation considered the mean activity per electrode
729 within a trial (converted into a vector), from visual stimulus presentation onset until the end of the
730 movement imagery interval (0 to 2000 ms). A third correlation analysis quantified the similarity of
731 spatiotemporal activity patterns across all stimulation-positive electrodes during a trial (-750 to
732 2000 ms). Group-level analysis considered the average correlation in each participant, where the
733 reliability of these correlations across the sample population was assessed using one-sample *t*-
734 tests. We report Bayes Factors (BF_{01}) for statistical tests evaluating evidence in favor of the null
735 hypothesis. Bayes Factors express the relative likelihood of the data under the models at hand and
736 were calculated using the JASP statistical software package (JASP Team, jasp-stats.org).
737 To assess whether the different neural phenomena were sensitive to the same sensorimotor
738 demands across individual movements, we performed representational similarity analysis on
739 temporal, spatial, and spatiotemporal activity patterns (Kriegeskorte, 2008). Instead of calculating
740 correlations between the neural phenomena directly, this approach calculates the similarity in
741 activity patterns between all possible trial combinations, resulting in a neural similarity matrix for
742 each phenomenon with as many rows and columns as there are trials. Given that the bottom-left
743 and top-right entries are identical in these matrices, we extracted only the top right entries
744 excluding the diagonals containing auto-correlations and converted these entries into vectors. Next,
745 second-order (Spearman) correlations of these trial-by-trial representational similarity vectors
746 quantified the similarity in sensitivity to sensorimotor demands between all combinations of neural
747 phenomena. This approach abstracts away from the activity patterns themselves such that
748 similarities in sensitivity to sensorimotor demands across different movements between
749 temporally or spatially non-overlapping neural phenomena can still be revealed. As above, the
750 reliability of these representational similarities across the sample population was assessed using
751 one-sample *t*-tests.
752

753 **Traveling wave analysis**

754 Alpha and beta traveling waves were identified as cortical signals showing systematic phase
755 variation across the electrode array (Ermentrout and Kleinfeld, 2001; Muller et al., 2018). We
756 filtered the time-domain data with a two-pass third-order zero-phase shift Butterworth at
757 individual alpha and beta frequency ranges determined using the four-step procedure outlined
758 above. We applied the Hilbert transform to extract the instantaneous phase of ongoing rhythmic
759 activity at each electrode and estimated for each instance of time (every ~2 ms) the spatial phase
760 gradient across the recording array. These spatial gradients represent distance-weighted phase
761 shifts between cortical signals at neighboring recording electrodes, where positive phase shifts
762 correspond to signals that have covered a greater distance along the unit circle and thus lead the
763 oscillation (Berens, 2009). To quantify traveling wave direction and velocities along the cortical
764 sheet, we projected and interpolated the phase data onto a two-dimensional plane defined by the
765 first two principal axes of the electrode array. This approach facilitates visualization and
766 interpretation of the subsequent gradient data and allows aggregating non-equidistant electrodes
767 from adjacent grid and strip arrays. Wave directionality was then found by calculating the angle
768 between spatial gradients estimated in both principal directions (1 cm in each direction). Wave
769 velocity was found by the ratio between the mean frequency of the rhythm and gradient magnitude.
770 To visualize the mean spatial progression of rhythmic activity across the electrode array, we
771 subtracted the instantaneous phase at a central sensorimotor reference electrode from each
772 electrode before averaging across trials and trial-time. We visualized the sample mean traveling
773 wave direction by projecting and averaging over each participant's probability distribution of
774 traveling wave directions onto the brain sagittal plane.

775 To assess whether the sensorimotor spatial gradients behaved like propagating waves at
776 the single-trial level, we computed the phase-gradient directionality (PGD) across all stimulation-
777 positive electrodes. PGD measures the degree of phase gradient alignment across an electrode
778 array, taking a range of values between 0 and 1, and is found by the ratio between the norm of the
779 mean spatial gradient and the mean gradient norm across the array (Rubino et al., 2006). We
780 assessed the reliability of the propagating waves by finding the mean PGD across trials and trial-
781 time and then comparing this value with two separate distributions of PGDs estimated from
782 randomly permuted time-points and randomly permuted electrode locations within the array. The
783 former redistributes activity over time, preserving the spatial structure of activity in sensorimotor
784 cortex, whereas the latter redistributes activity over space, preserving the temporal structure of
785 activity in a trial. Rayleigh tests of uniformity were used to determine whether the traveling

786 sensorimotor waves moved in a consistent direction across trials and trial-time (Fisher, 1995). To
787 assess the consistency of wave propagation direction at a given time and electrode, we computed
788 the directional consistency (DC). DC measures the degree of consistency in phase gradient
789 direction, taking a range of values between 0 and 1, and is found by the mean resultant vector
790 length across trials (Zhang et al., 2018).
791
792

Author contributions

A.S., L.B., F.P.L, and I.T. conceived and designed the study. L.B. conducted the study and collected the data. A.S., L.B., and I.T. conducted the data analyses and drafted the manuscript. M.V., E.A., F.S.S.L., C.H.D., R.T.K, and F.P.L. provided critical revisions. All authors approved the final version of the manuscript.

Data and code availability

Analysis code for spectral features extraction from the electrophysiological data are published as supplementary data.

Acknowledgments

The authors thank the patients and their families for their participation and A. Bastos, C. W. Hoy, and R. Oostenveld for invaluable discussions and comments on previous versions of this article. A.S. was supported by Rubicon grant 446-14-007 from NWO and Marie Sklodowska-Curie Global Fellowship 658868 from the European Union. L.B. was supported by Brain and Cognition grant 433-09-248 from NWO awarded to I.T.

REFERENCES

Alayrangues J, Torrecillos F, Jahani A, Malfait N. 2019. Error-related modulations of the sensorimotor post-movement and foreperiod beta-band activities arise from distinct neural substrates and do not reflect efferent signal processing. *Neuroimage* **184**:10–24.

Bahramisharif A, van Gerven MAJ, Aarnoutse EJ, Mercier MR, Schwartz TH, Foxe JJ, Ramsey NF, Jensen O. 2013. Propagating neocortical gamma bursts are coordinated by traveling alpha waves. *J Neurosci* **33**:18849–18854.

Baker SN, Olivier E, Lemon RN. 1997. Coherent oscillations in monkey motor cortex and hand muscle EMG show task-dependent modulation. *J Physiol* **501 (Pt 1)**:225–241.

Bastos AM, Briggs F, Alitto HJ, Mangun GR, Usrey WM. 2014. Simultaneous recordings from the primary visual cortex and lateral geniculate nucleus reveal rhythmic interactions and a cortical source for γ-band oscillations. *J Neurosci* **34**:7639–7644.

Bastos AM, Loonis R, Kornblith S, Lundqvist M, Miller EK. 2018. Laminar recordings in frontal cortex suggest distinct layers for maintenance and control of working memory. *Proc Natl Acad Sci U S A* **115**:1117–1122.

Berens P. 2009. CircStat: AMATLABToolbox for Circular Statistics. *J Stat Softw* **31**. doi:10.18637/jss.v031.i10

Berger H. 1938. Über das Elektrenkephalogramm des Menschen. *Archiv für Psychiatrie und Nervenkrankheiten*. doi:10.1007/bf01824101

Bressler SL, Richter CG. 2015. Interareal oscillatory synchronization in top-down neocortical processing. *Curr Opin Neurobiol* **31**:62–66.

Brinkman L, Stolk A, Dijkerman HC, de Lange FP, Toni I. 2014. Distinct roles for alpha- and beta-band oscillations during mental simulation of goal-directed actions. *J Neurosci* **34**:14783–14792.

Brinkman L, Stolk A, Marshall TR, Esterer S, Sharp P, Dijkerman HC, de Lange FP, Toni I. 2016. Independent Causal Contributions of Alpha- and Beta-Band Oscillations during Movement Selection. *J Neurosci* **36**:8726–8733.

Brovelli A, Ding M, Ledberg A, Chen Y, Nakamura R, Bressler SL. 2004. Beta oscillations in a large-scale sensorimotor cortical network: directional influences revealed by Granger causality. *Proc Natl Acad Sci U S A* **101**:9849–9854.

Bruno AM, Frost WN, Humphries MD. 2015. Modular deconstruction reveals the dynamical and physical building blocks of a locomotion motor program. *Neuron* **86**:304–318.

Carlqvist H, Nikulin VV, Strömberg JO, Brismar T. 2005. Amplitude and phase relationship between alpha and beta oscillations in the human electroencephalogram. *Med Biol Eng Comput* **43**:599–607.

Cisek P, Kalaska JF. 2004. Neural correlates of mental rehearsal in dorsal premotor cortex. *Nature* **431**:993–996.

Crone NE, Miglioretti DL, Gordon B, Sieracki JM, Wilson MT, Uematsu S, Lesser RP. 1998. Functional mapping of human sensorimotor cortex with electrocorticographic spectral analysis. I. Alpha and beta event-related desynchronization. *Brain* **121 (Pt 12)**:2271–2299.

Cuevas K, Cannon EN, Yoo K, Fox NA. 2014. The Infant EEG Mu Rhythm: Methodological Considerations and Best Practices. *Dev Rev* **34**:26–43.

Dale AM, Fischl B, Sereno MI. 1999. Cortical surface-based analysis. I. Segmentation and surface reconstruction. *Neuroimage* **9**:179–194.

de Lange FP, Helmich RC, Toni I. 2006. Posture influences motor imagery: an fMRI study. *Neuroimage* **33**:609–617.

de Lange FP, Jensen O, Bauer M, Toni I. 2008. Interactions between posterior gamma and frontal alpha/beta oscillations during imagined actions. *Front Hum Neurosci* **2**:7.

Dombeck DA, Graziano MS, Tank DW. 2009. Functional clustering of neurons in motor cortex determined by cellular resolution imaging in awake behaving mice. *J Neurosci* **29**:13751–13760.

Ebbesen CL, Brecht M. 2017. Motor cortex - to act or not to act? *Nat Rev Neurosci* **18**:694–705.

Elsayed GF, Lara AH, Kaufman MT, Churchland MM, Cunningham JP. 2016. Reorganization between preparatory and movement population responses in motor cortex. *Nat Commun* **7**:13239.

Ermentrout GB, Kleinfeld D. 2001. Traveling electrical waves in cortex: insights from phase dynamics and speculation on a computational role. *Neuron* **29**:33–44.

Fisher NI. 1995. Statistical Analysis of Circular Data. Cambridge University Press.

Fransen AMM, Dimitriadis G, van Ede F, Maris E. 2016. Distinct α- and β-band rhythms over rat somatosensory cortex with similar properties as in humans. *J Neurophysiol* **115**:3030–3044.

Gao R, Peterson EJ, Voytek B. 2017. Inferring synaptic excitation/inhibition balance from field potentials. *Neuroimage* **158**:70–78.

Gentili R, Cahouet V, Ballay Y, Papaxanthis C. 2004. Inertial properties of the arm are accurately predicted during motor imagery. *Behav Brain Res* **155**:231–239.

Graziano MSA. 2016. Ethological Action Maps: A Paradigm Shift for the Motor Cortex. *Trends Cogn Sci* **20**:121–132.

Greenhouse I, Sias A, Labruna L, Ivry RB. 2015. Nonspecific Inhibition of the Motor System during Response Preparation. *J Neurosci* **35**:10675–10684.

Greve DN, Van der Haegen L, Cai Q, Stufflebeam S, Sabuncu MR, Fischl B, Brysbaert M. 2013. A surface-based analysis of language lateralization and cortical asymmetry. *J Cogn Neurosci* **25**:1477–1492.

Haegens S, Cousijn H, Wallis G, Harrison PJ, Nobre AC. 2014. Inter- and intra-individual variability in alpha peak frequency. *Neuroimage* **92**:46–55.

Halgren M, Ulbert I, Bastuji H, Fabo D, Eross L, Rey M, Devinsky O, Doyle WK, Mak-McCully R, Halgren E, Wittner L, Chauvel P, Heit G, Eskandar E, Mandell A, Cash SS. 2017. The Generation and Propagation of the Human Alpha Rhythm. doi:10.1101/202564

Hari R. 2006. Action-perception connection and the cortical mu rhythm. *Prog Brain Res* **159**:253–260.

He BJ. 2014. Scale-free brain activity: past, present, and future. *Trends Cogn Sci* **18**:480–487.

Heitmann S, Boonstra T, Breakspear M. 2013. A dendritic mechanism for decoding traveling waves: principles and applications to motor cortex. *PLoS Comput Biol* **9**:e1003260.

Hermes D, Miller KJ, Noordmans HJ, Vansteensel MJ, Ramsey NF. 2010. Automated electrocorticographic electrode localization on individually rendered brain surfaces. *J Neurosci Methods* **185**:293–298.

Jasper H, Penfield W. 1949. Electrocorticograms in man: Effect of voluntary movement upon the electrical activity of the precentral gyrus. *Archiv f□r Psychiatrie und Nervenkrankheiten* **183**:163–174.

Johnston K, Ma L, Schaeffer L, Everling S. 2019. Alpha-oscillations modulate preparatory activity in marmoset area 8Ad. *J Neurosci*. doi:10.1523/JNEUROSCI.2703-18.2019

Jones SR. 2016. When brain rhythms aren't "rhythmic": implication for their mechanisms and meaning. *Curr Opin Neurobiol* **40**:72–80.

Jurkiewicz MT, Gaetz WC, Bostan AC, Cheyne D. 2006. Post-movement beta rebound is generated in motor cortex: evidence from neuromagnetic recordings. *Neuroimage* **32**:1281–1289.

Kriegeskorte N. 2008. Representational similarity analysis – connecting the branches of systems neuroscience. *Front Syst Neurosci*. doi:10.3389/neuro.06.004.2008

Kriegeskorte N, Goebel R, Bandettini P. 2006. Information-based functional brain mapping. *Proc Natl Acad Sci U S A* **103**:3863–3868.

Kühn AA, Doyle L, Pogosyan A, Yarrow K, Kupsch A, Schneider G-H, Hariz MI, Trottenberg T, Brown P. 2006. Modulation of beta oscillations in the subthalamic area during motor imagery in

907 Parkinson's disease. *Brain* **129**:695–706.
908 Lachaux J-P, Axmacher N, Mormann F, Halgren E, Crone NE. 2012. High-frequency neural activity
909 and human cognition: past, present and possible future of intracranial EEG research. *Prog*
910 *Neurobiol* **98**:279–301.
911 Lebon F, Ruffino C, Greenhouse I, Labruna L, Ivry RB, Papaxanthis C. 2019. The Neural Specificity of
912 Movement Preparation During Actual and Imagined Movements. *Cereb Cortex* **29**:689–700.
913 Lendner JD, Helfrich RF, Mander BA, Romundstad L, Lin JJ, Walker MP, Larsson PG, Knight RT. n.d.
914 An Electrophysiological Marker of Arousal Level in Humans. doi:10.1101/625210
915 Leszczynski M, Barczak A, Kajikawa Y, Ulbert I, Falchier A, Tal I, Haegens S, Melloni L, Knight R,
916 Schroeder C. n.d. Dissociation of broadband high-frequency activity and neuronal firing in the
917 neocortex. doi:10.1101/531368
918 Leventhal DK, Gage GJ, Schmidt R, Pettibone JR, Case AC, Berke JD. 2012. Basal ganglia beta
919 oscillations accompany cue utilization. *Neuron* **73**:523–536.
920 Little S, Bonaiuto J, Barnes G, Bestmann S. n.d. Motor cortical beta transients delay movement
921 initiation and track errors. doi:10.1101/384370
922 Madsen M, Takemi M, Kesselheim J, Tashiro S, Siebner H. 2019. Focal TACS of the primary motor
923 hand area at individual mu and beta rhythm – effects on cortical excitability. *Brain Stimulation*.
924 doi:10.1016/j.brs.2018.12.896
925 Manning JR, Jacobs J, Fried I, Kahana MJ. 2009. Broadband shifts in local field potential power
926 spectra are correlated with single-neuron spiking in humans. *J Neurosci* **29**:13613–13620.
927 Maris E, Oostenveld R. 2007. Nonparametric statistical testing of EEG- and MEG-data. *J Neurosci*
928 *Methods* **164**:177–190.
929 Miller KJ, Schalk G, Fetz EE, den Nijs M, Ojemann JG, Rao RPN. 2010. Cortical activity during motor
930 execution, motor imagery, and imagery-based online feedback. *Proc Natl Acad Sci U S A*
931 **107**:4430–4435.
932 Miller KJ, Sorensen LB, Ojemann JG, den Nijs M. 2009. Power-law scaling in the brain surface
933 electric potential. *PLoS Comput Biol* **5**:e1000609.
934 Mima T, Hallett M. 1999. Electroencephalographic analysis of cortico-muscular coherence:
935 reference effect, volume conduction and generator mechanism. *Clin Neurophysiol* **110**:1892–
936 1899.
937 Mink JW. 1996. The basal ganglia: focused selection and inhibition of competing motor programs.
938 *Prog Neurobiol* **50**:381–425.
939 Muller L, Chavane F, Reynolds J, Sejnowski TJ. 2018. Cortical travelling waves: mechanisms and
940 computational principles. *Nat Rev Neurosci* **19**:255–268.
941 Oostenveld R, Fries P, Maris E, Schoffelen J-M. 2011. FieldTrip: Open source software for advanced
942 analysis of MEG, EEG, and invasive electrophysiological data. *Comput Intell Neurosci*
943 **2011**:156869.
944 Pfurtscheller G, Berghold A. 1989. Patterns of cortical activation during planning of voluntary
945 movement. *Electroencephalogr Clin Neurophysiol* **72**:250–258.
946 Picazio S, Veniero D, Ponzo V, Caltagirone C, Gross J, Thut G, Koch G. 2014. Prefrontal control over
947 motor cortex cycles at beta frequency during movement inhibition. *Curr Biol* **24**:2940–2945.
948 Ray S, Maunsell JHR. 2011. Different origins of gamma rhythm and high-gamma activity in macaque
949 visual cortex. *PLoS Biol* **9**:e1000610.
950 Rich EL, Wallis JD. 2017. Spatiotemporal dynamics of information encoding revealed in
951 orbitofrontal high-gamma. *Nat Commun* **8**:1139.
952 Rosenbaum DA, Loukopoulos LD, Meulenbroek RG, Vaughan J, Engelbrecht SE. 1995. Planning
953 reaches by evaluating stored postures. *Psychol Rev* **102**:28–67.
954 Rubino D, Robbins KA, Hatsopoulos NG. 2006. Propagating waves mediate information transfer in
955 the motor cortex. *Nat Neurosci* **9**:1549–1557.
956 Saleh M, Reimer J, Penn R, Ojakangas CL, Hatsopoulos NG. 2010. Fast and slow oscillations in human

primary motor cortex predict oncoming behaviorally relevant cues. *Neuron* **65**:461–471.
Salmelin R, Hari R. 1994. Characterization of spontaneous MEG rhythms in healthy adults. *Electroencephalogr Clin Neurophysiol* **91**:237–248.
Schreckenberger M, Lange-Asschenfeldt C, Lochmann M, Mann K, Siessmeier T, Buchholz H-G, Bartenstein P, Gründer G. 2004. The thalamus as the generator and modulator of EEG alpha rhythm: a combined PET/EEG study with lorazepam challenge in humans. *Neuroimage* **22**:637–644.
Shenoy KV, Sahani M, Churchland MM. 2013. Cortical control of arm movements: a dynamical systems perspective. *Annu Rev Neurosci* **36**:337–359.
Stolk A, Griffin S, van der Meij R, Dewar C, Saez I, Lin JJ, Piantoni G, Schoffelen J-M, Knight RT, Oostenveld R. 2018. Integrated analysis of anatomical and electrophysiological human intracranial data. *Nat Protoc*. doi:10.1038/s41596-018-0009-6
Szurhaj W, Derambure P, Labyt E, Cassim F, Bourriez J-L, Isnard J, Guieu J-D, Mauguière F. 2003. Basic mechanisms of central rhythms reactivity to preparation and execution of a voluntary movement: a stereoelectroencephalographic study. *Clin Neurophysiol* **114**:107–119.
Takahashi K, Kim S, Coleman TP, Brown KA, Suminski AJ, Best MD, Hatsopoulos NG. 2015. Large-scale spatiotemporal spike patterning consistent with wave propagation in motor cortex. *Nat Commun* **6**:7169.
Tan H, Wade C, Brown P. 2016. Post-Movement Beta Activity in Sensorimotor Cortex Indexes Confidence in the Estimations from Internal Models. *J Neurosci* **36**:1516–1528.
Tiihonen J, Kajola M, Hari R. 1989. Magnetic mu rhythm in man. *Neuroscience*. doi:10.1016/0306-4522(89)90299-6
Toro C, Deuschl G, Thatcher R, Sato S, Kufta C, Hallett M. 1994. Event-related desynchronization and movement-related cortical potentials on the ECoG and EEG. *Electroencephalogr Clin Neurophysiol* **93**:380–389.
van Elswijk G, Maij F, Schoffelen J-M, Overeem S, Stegeman DF, Fries P. 2010. Corticospinal beta-band synchronization entails rhythmic gain modulation. *J Neurosci* **30**:4481–4488.
van Kerkoerle T, Self MW, Dagnino B, Gariel-Mathis M-A, Poort J, van der Togt C, Roelfsema PR. 2014. Alpha and gamma oscillations characterize feedback and feedforward processing in monkey visual cortex. *Proc Natl Acad Sci U S A* **111**:14332–14341.
Vansteensel MJ, Bleichner MG, Dintzner LT, Aarnoutse EJ, Leijten FSS, Hermes D, Ramsey NF. 2013. Task-free electrocorticography frequency mapping of the motor cortex. *Clin Neurophysiol* **124**:1169–1174.
van Wijk BCM, Beek PJ, Daffertshofer A. 2012. Neural synchrony within the motor system: what have we learned so far? *Front Hum Neurosci* **6**:252.
Vargas CD, Olivier E, Craighero L, Fadiga L, Duhamel JR, Sirigu A. 2004. The Influence of Hand Posture on Corticospinal Excitability during Motor Imagery: A Transcranial Magnetic Stimulation Study. *Cerebral Cortex*. doi:10.1093/cercor/bhh080
Wen H, Liu Z. 2015. Separating Fractal and Oscillatory Components in the Power Spectrum of Neurophysiological Signal. *Brain Topogr* **29**:13–26.
West TO, Berthouze L, Halliday DM, Litvak V, Sharott A, Magill PJ, Farmer SF. 2018. Propagation of beta/gamma rhythms in the cortico-basal ganglia circuits of the parkinsonian rat. *J Neurophysiol* **119**:1608–1628.
Zhang H, Watrous AJ, Patel A, Jacobs J. 2018. Theta and Alpha Oscillations Are Traveling Waves in the Human Neocortex. *Neuron* **98**:1269–1281.e4.

1005

Supporting Information

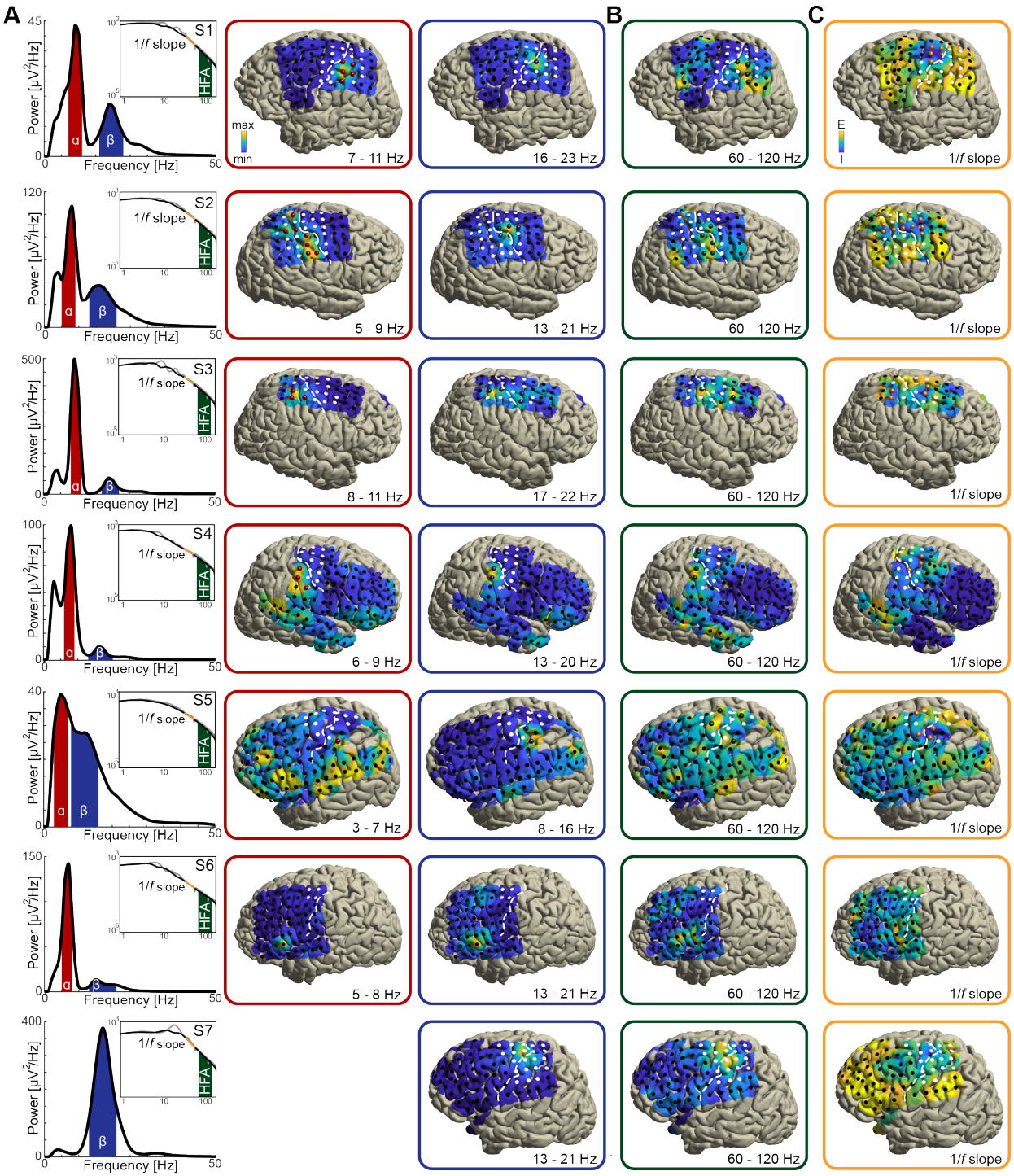

Supplemental Figure 1. As in Figure 2A-C, for seven individuals with sensorimotor coverage. Participant S7 lacked a rhythmic power-spectral component in the alpha frequency range (around 8 - 12 Hz; see bottom left power-spectrum in A) and was excluded from further analysis.

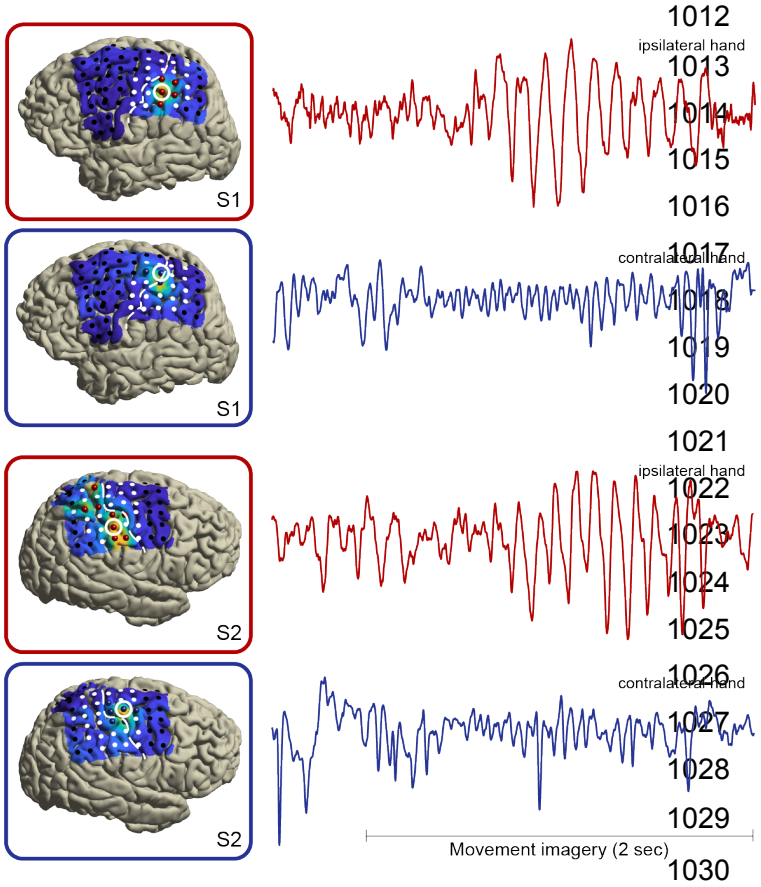

Supplemental Figure 2. Single-trial broadband/unfiltered cortical signals from alpha- and beta-band local maxima (highlighted red and blue electrodes, respectively) in two representative individuals. It can be seen that the group-level power dynamics in Figure 2E, showing attenuated beta rhythmic activity in contralateral somatomotor cortex and enhanced alpha rhythmic activity in ipsilateral somatosensory cortex during movement imagery, are preserved on the single-trial level of individuals. Further note that both rhythm types are sustained for many cycles.

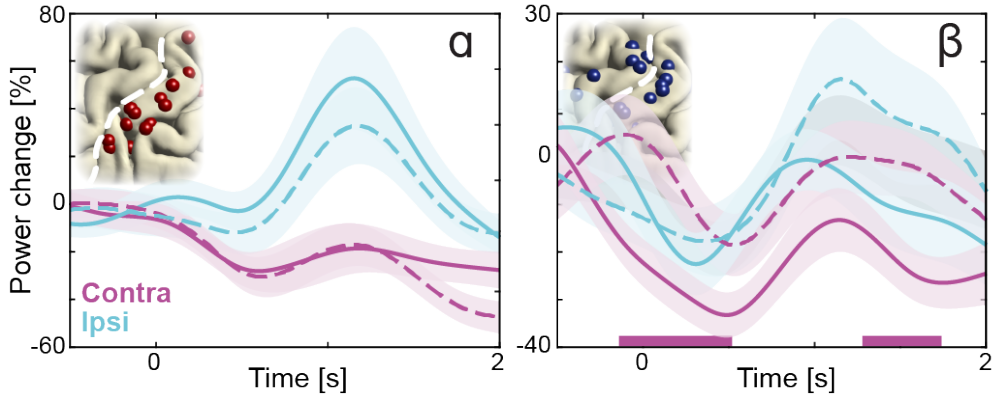

Supplemental Figure 3. As in Figure 2E, but with mean temporal dynamics of high demand trials (solid lines, cylinder orientations that afforded both overhand and underhand grasping) and low demand trials (dashed lines, cylinder orientations that afforded grasping in a single manner only). The direction of the effects is consistent with a previous magnetoencephalography study showing that as movement demands increased, alpha-band power increased in the sensorimotor cortex ipsilateral to the arm used for motor imagery, whereas beta-band power concurrently decreased in the contralateral sensorimotor cortex. Colored bars along the x-axes indicate time intervals of statistically significant task demand effects.

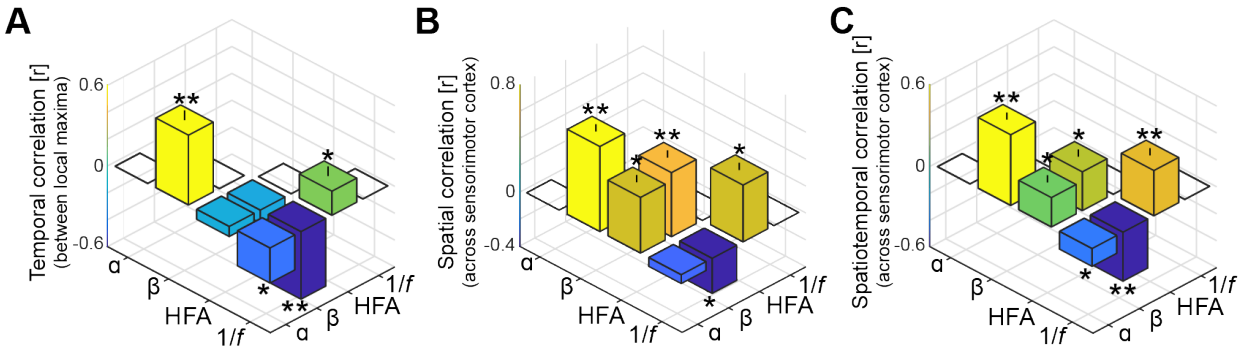

Supplemental Figure 4. As in Figure 3A-C, but without accounting for shared variance in alpha- and beta-band frequency bands originating from concurrent 1/*f* modulations in the power-spectrum. It can be seen from the leftmost bars in these figures that without the separation of rhythmic and arrhythmic activity in the power-spectrum, alpha- and beta-band rhythms appear temporally and spatially correlated.

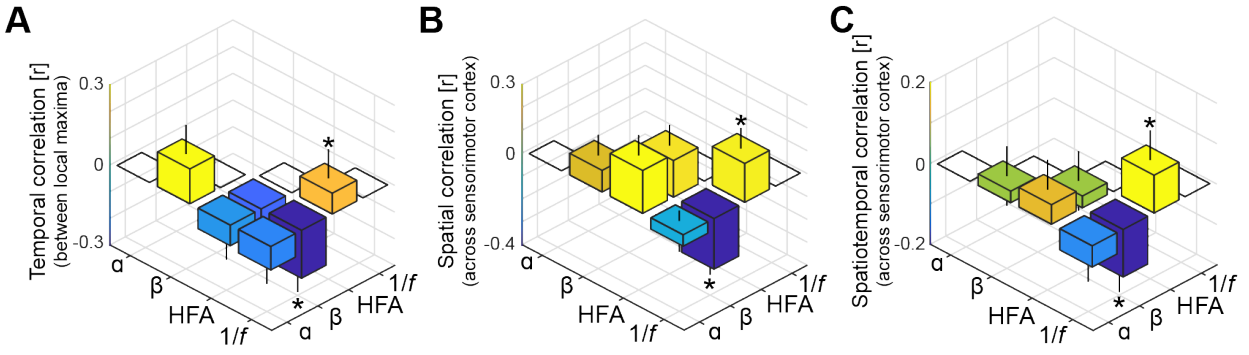

Supplemental Figure 5. As in Figure 3A-C, but with high-frequency activity and the 1/*f* slope index based on the rhythmic component rather than on the arrhythmic component of the power-spectrum. It can be seen that interactions involving low-frequency phenomena (alpha- and beta-band rhythmic activity) and local excitability metrics (high-frequency activity and the 1/*f* slope) are substantially weaker compared to the original correlations shown in Figure 3, despite that all spectral features are based on the same rhythmic component of the power-spectrum.

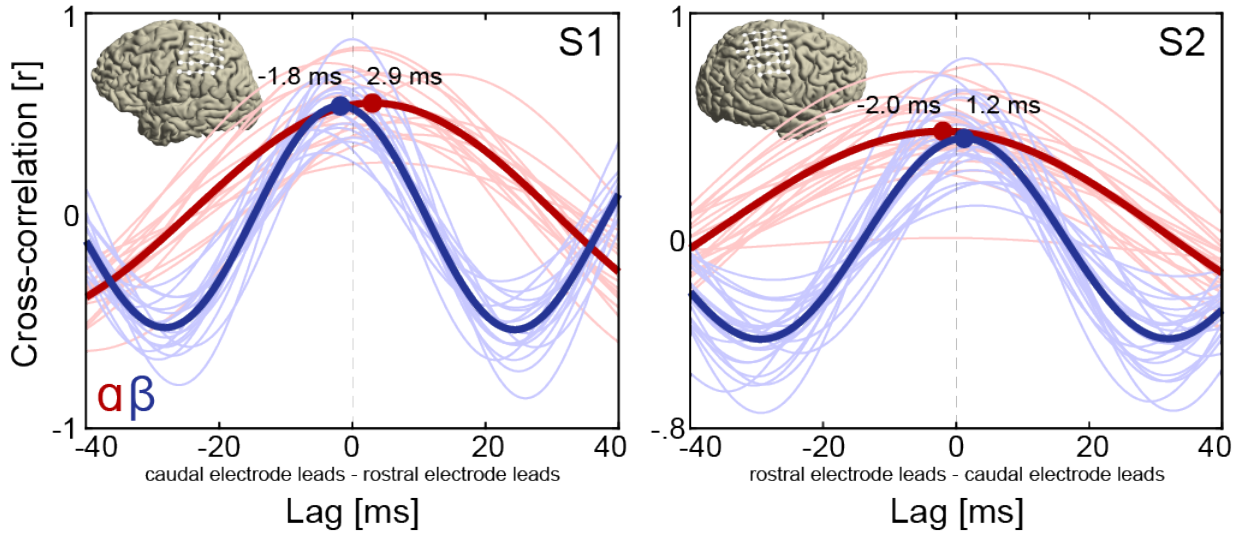

Supplemental Figure 6. Cross-correlation functions of alpha and beta rhythmic activity at rostro-caudal electrode pairs on the sensorimotor cortex of two representative individuals. It can be seen that rostral electrodes led caudal electrodes in the alpha frequency range during movement imagery (red lines), consistent with alpha waves traveling in a rostral direction. Conversely, caudal electrodes led rostral electrodes in the beta frequency range (blue lines), consistent with beta waves traveling in a caudal direction. This pattern of directionality is consistent with the instantaneous phase-based representations in Figure 4, showing concurrent alpha and beta waves traveling along opposite directions during movement imagery. Thin lines indicate mean cross-correlation functions across trials at individual electrode pairs. Thick lines indicate mean cross-correlation functions across all electrode pairs. White markers and lines on the brain insets indicate rostro-caudal electrode pairs on which amplitude-based cross-correlations were based. All lags were statistically significant (see Supplemental Analyses for details). Note that rostro-caudal direction is flipped on the x-axis of participant S2.

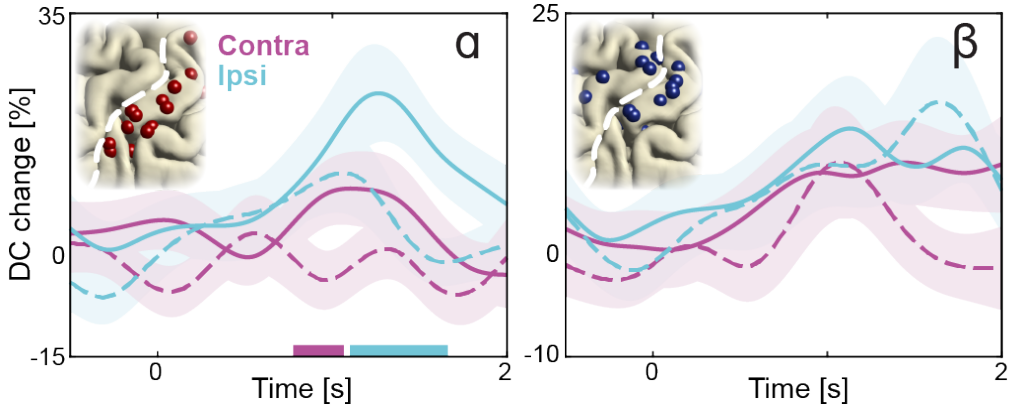

Supplemental Figure 7. As in Figure 4D, but with directional consistency of wave propagation for high demand trials (solid lines, cylinder orientations that afforded both overhand and underhand grasping) and

for low demand trials (dashed lines, cylinder orientations that afforded grasping in a single manner only). Alpha waves propagated more consistently through alpha-band local maxima during imagined movement on high demand trials. Colored bars along the x-axes indicate time intervals of statistically significant task demand effects.

Supplemental Movie 1. Time-lapse movie of concurrent traveling alpha and beta waves in participant S1 during movement imagery. Cortical phase maps indicate the average phase at each cortical site relative to a central sensorimotor reference electrode. Small cone-shaped arrows indicate the mean propagation direction at each stimulation-positive electrode, with arrow size weighted by the local phase gradient magnitude. Large arrows indicate the mean propagation direction across sensorimotor cortex, with arrow size weighted by the alignment of sensorimotor gradients (phase gradient directionality, PGD). Time is in seconds after cylinder appearance.

Supplemental Movie 2. As in Movie 1, for participant S2.

Supplemental Data. Analysis code for the extraction of spectral features from the electrophysiological signal.

Supplemental Analyses. Several control analyses were performed to test for alternative interpretations of the findings obtained with the IRASA technique and the 1/*f* slope index. First, the main analysis considering spectral features obtained using the IRASA technique revealed uncorrelated alpha and beta rhythmic activity in sensorimotor cortex. We performed an additional analysis testing whether power in the two frequency bands is also uncorrelated when broadband 1/*f* components of the signal are not accounted for, i.e., using the original power-spectra. It can be seen from the leftmost bars in Figure S4 that performing the same correlation analysis on the original power-spectra yielded strong temporal and spatial correlations between alpha- and beta-band power. This observation underscores the importance of accounting for shared variance in alpha and beta power envelopes originating from broadband 1/*f* modulations. Second, the main analysis investigating the influence of rhythmic activity on local excitability found that the slope of the arrhythmic 1/*f* component had a differential relationship with alpha and beta rhythmic activity during movement imagery. It could be argued that the relation between beta rhythmic activity and the 1/*f* slope was artificially stronger because of the beta-band being closer than the alpha-band to the 30-50 Hz band of the power-spectrum on which the 1/*f* slope index is based. Accordingly, we performed an additional analysis grounded on the idea that a spurious interaction between beta-band power and the steepness of the 1/*f* slope should be amplified when both spectral features are directly based on the same (rhythmic) component of the power-spectrum, resulting in stronger correlations. As can be seen from Figure S5, correlations between beta-band power and the steepness of the 1/*f* slope were substantially reduced with both features based on the same component, compared to the original correlations shown in Figure 3. This observation indicates that the reciprocal

changes between beta rhythmic activity and the slope of the arrhythmic $1/f$ component cannot be readily explained by a spurious relationship between these two spectral features.

Several other control analyses were performed to examine further the robustness and functional relevance of alpha and beta traveling waves. First, it could be argued that the traveling wave analyses depended on relatively noise-sensitive instantaneous estimates of phase and subsequent circular statistics. Accordingly, we performed an additional analysis that considered the entire time-series of alpha and beta rhythmic activity during movement imagery. Following insight from our phase-based analyses, showing activity moving along a rostro-caudal direction across the frontoparietal cortex, we calculated amplitude-based cross-correlations between electrode pairs aligned with the rostro-caudal axis in two representative individuals (see the brain insets in Figure S6). We rejected electrode pairs with cross-correlation functions explaining less than 50% of the mean distribution of cross-correlation in the sensorimotor cortex, based on leave-one-out cross-validation (1 and 3 alpha-band cross-correlation functions were held out in participants S1 and S2, respectively). This analysis showed that rostral electrodes led caudal electrodes in the alpha frequency range (red lines in Figure S6), consistent with alpha waves traveling in a rostral direction. Conversely, caudal electrodes led rostral electrodes in the beta frequency range (blue lines in the same figure), consistent with beta waves traveling in a caudal direction ($p < 0.001$ for all lags, estimated from shuffled data using one-sample t-tests). This pattern of directionality is consistent with the instantaneous phase-based representations in Figure 4, showing concurrent alpha and beta waves traveling along opposite directions during movement imagery. Second, we examined whether the task-relevant traveling waves were additionally sensitive to selection demands during movement imagery. To this end, we examined the directional consistency (DC) of those waves, which measures the degree of consistency across trials in the phase-gradient direction. In the main analysis, it was found that alpha waves traveled more consistently through alpha-band local maxima ipsilateral to the selected arm during movement imagery, as compared to baseline levels (Figure 4D). As seen in Figure S7, alpha waves propagated even more consistently through alpha-band local maxima during imagined movement of high demand trials, as compared to low demand trials. This effect occurred around the same time as alpha-band power increased during imagined movement of the ipsilateral hand (Figure 2E), particularly when selection demands were high (Figure S3). Taken together, these additional observations are consistent with the main findings of the study. Alpha and beta rhythm-dependent (dis)inhibition is task-relevant and propagated in a consistent spatiotemporal pattern.